Acta Geotechnica
DOI 10.1007/s11440-011-0152-5

RESEARCH PAPER

Experimental and discrete element modeling studies of the trapdoor problem: influence of the macro-mechanical frictional parameters

B. Chevalier · G. Combe · P. Villard

Received: 30 May 2011 / Accepted: 22 November 2011

Abstract Granular soils have the inherent ability to develop load transfers in their mass. Mechanisms of load transfers are used as a basic principle of many civil and geotechnical engineering applications. However, their complexity makes it difficult to formulate relevant design methods for such works. The trapdoor problem is one of the ways to reproduce load transfers by the arching effect in a granular layer in non-complex conditions. In addition, many analytical solutions for the prediction of load transfer mechanisms are based on the trapdoor problem. However, some of the parameters required are still being widely discussed, in particular the ratio of horizontal stress to vertical stress. For this paper, an experimental device for trapdoor tests in plane strain conditions was created and several geomaterials were tested. Three phases in the response of the materials were consistently observed. Each of these phases corresponded to a specific displacement of the trapdoor. A first phase of high load transfer was observed followed by a transition phase which was followed by a critical phase for which the load transfer amplitude increased and stabilized. Analytical solutions and experimental values of load transfers were compared. Considerable differences between the stress ratio needed to fit the experimental data and the stress ratio proposed in the analytical models were noted. Based on the conclusions of the experimental study, the discrete element method was used to model the same trapdoor problem. A wide range of granular materials was modeled and tested in the trapdoor problem. The three phases in the response of the layer were also observed in the numerical modeling. In addition, it was shown that the shear strength of the material is the key parameter of load transfers: peak shear resistance for the small displacements of the trapdoor and critical shear strength for the larger displacements. A micro-mechanical analysis showed that the effective stress ratio in the sheared zone does not vary as much with shear strength. Stress ratios here were again greater than those proposed in the analytical solutions. Nevertheless, the relevance of the solution of Terzaghi was confirmed as soon as the stress ratio was correctly chosen.

B. Chevalier (✉) · G. Combe · P. Villard
UJF-Grenoble 1, Grenoble-INP, CNRS UMR 5521,
3SR Lab, B.P. 53, 38041 Grenoble Cedex 09, France
e-mail: bastien.chevalier@polytech.univ-bpclermont.fr

G. Combe
e-mail: gael.combe@ujf-grenoble.fr

P. Villard
e-mail: pascal.villard@ujf-grenoble.fr

Present Address:
B. Chevalier
Clermont Université, Université Blaise Pascal,
Institut Pascal, BP 10448, 63000 Clermont-Ferrand, France

B. Chevalier
CNRS, UMR 6602, Institut Pascal, 63171 Aubiere, France

Keywords Discrete element method · Friction angle · Granular materials · Load transfer · Trapdoor problem

1 Introduction

Numerous civil and geotechnical engineering applications involve the use of granular layers that play a specific role in the distribution of the forces caused by the weight of the superstructure and any overloads applied. For example, in the technique of reinforcement of soft soil by rigid inclusions, a granular layer located over the piles is used to increase the load supported by the piles and consequently to decrease the load acting on the supporting soil and subsequently surface settlement [12]. In the case of embankments reinforced with basal geosynthetic sheeting on soft soils [28], the granular material used for the embankment construction creates an arching effect over sinkhole cavities, thereby reducing the load applied to the reinforcement and thus limiting surface settlement [43]. Several codes of practice operate on the observations made on the trapdoor problem to estimate the loads acting on buried structures and resulting from a vertical displacement of a granular mass moving between fixed parts of material. This is the case for flexible ditch conduits [1], for geosynthetic sheets used as reinforcements in subsidence areas [7, 19] or for tunnel-boring machines.

In order to improve the behavior of these structures, a tri-dimensional numerical model based on the discrete element method (DEM) was developed. To test the ability of the numerical model to describe the load transfer mechanisms, numerical and experimental studies in plane strain conditions of the trapdoor problem were carried out.

The trapdoor problem [40, 41] consists in moving vertically a trapdoor located at the basis of a granular layer (Fig. 1). During the tests, the pressure acting on the trapdoor decreases due to load transfers occurring in the granular material. Load transfers are the consequences of intergranular rearrangements and modifications of the orientations of contact forces according to the pattern of an arch above the trapdoor. This problem is similar to the study of the pressures in silos, described analytically by Janssen [25], where the pressure p acting at the bottom of a silo of width $2B$ filled with a granular material of density γ, is given by

$$p = \frac{B\gamma}{K \tan\phi}\left(1 - e^{-(Kh/B)\tan\phi}\right) \tag{1}$$

where K represents the ratio of horizontal stress to vertical stress on or near the walls of the silo, ϕ the friction angle between the granular material and the walls and h the height of the granular material in the silo. For the specific case of pressure in silos, the coefficient K has been

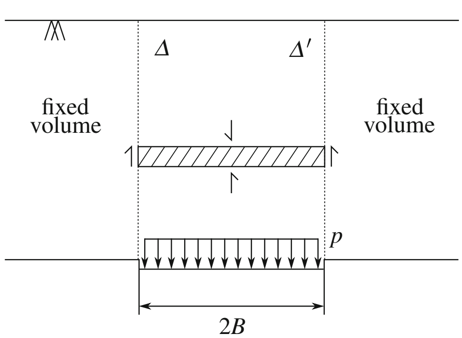

Fig. 1 Description of the trapdoor problem

discussed by many authors in the past decades [25, 26, 44, 45].

Terzaghi [40] extended this analytical solution to the trapdoor problem by studying the equilibrium of forces on a horizontal layer of soil located above the trapdoor. Thus, the boundaries represented by the walls in the silo problem are replaced by two vertical planes (Δ and Δ' in Fig. 1) starting at each edge of the trapdoor.

The difficulty in this analytical solution lies in the determination of the following two values ϕ and K:

- in the special case of the trapdoor problem, the angle of friction ϕ should be obtained in plane strain conditions and, depending on the amplitude of the trapdoor displacement, for lesser or greater strains,
- the stress ratio K is itself linked to ϕ.

For K, there are several propositions based on different assumptions concerning the behavior of the granular material at the boundaries between the soil located just above the trapdoor and the remainder of the material. Marston and Anderson [29] used an analytical solution similar to Eq. 1 for predicting the pressure acting on concrete pipes taking into account a stress ratio K equal to the active earth pressure coefficient [33].

$$K = K_a = \frac{1 - \sin\phi}{1 + \sin\phi} \tag{2}$$

The definition of the stress ratio $K = \sigma_x/\sigma_z$ equal to the active earth pressure coefficient K_a implies that σ_x and σ_z correspond to the principal stresses. Handy [23] pointed out that this assumption is not compatible with the existence of vertical tangential stresses and he proposed another stress ratio resulting from the equilibrium of a catenary shaped stratum. This new assumption implies that the principal stress directions differ from the vertical and horizontal directions. The new stress ratio K_w [30] is defined by

$$K = K_w = 1.06\left[\cos^2\left(\frac{\pi}{4} + \frac{\phi}{2}\right) + K_a \sin^2\left(\frac{\pi}{4} + \frac{\phi}{2}\right)\right] \tag{3}$$

Other solutions exist for the stress ratio, notably based on the theory of shear banding. For example, Vardoulakis [42] considered the two vertical planes (Δ and Δ' on Fig. 1) as a zone of localization of the shear strains: two different stress ratios were proposed, each associated with a value of the friction angle ϕ of the material within the shear band. Corresponding to the Coulomb solution, the first of these is

$$\phi = \phi_c \tag{4}$$

where ϕ_c is the critical friction angle of the granular material. The second value of the estimated friction angle within the shear band is given by Roscoe [34] and is defined by

$$\tan\phi = \sin\phi_c \tag{5}$$

Vardoulakis defines a stress ratio K_v depending on the inclination β of the minor principal stress at the outer edge of the shear band going in the opposite direction to the shear band:

$$K = K_v = \frac{1 - \sin\phi_c \cos 2(\pi/2 + \beta)}{1 + \sin\phi_c \cos 2(\pi/2 + \beta)} \tag{6}$$

where β is defined by

$$\tan\beta = \lambda_e - \sqrt{\lambda_e^2 - \lambda^2} \tag{7}$$

with

$$\lambda_e = \frac{\sin\phi_c}{\tan\phi(1 - \sin\phi_c)} \tag{8}$$

$$\lambda = \tan\left(\frac{\pi}{4} + \frac{\phi_c}{2}\right) \tag{9}$$

If the minor principal stress direction is perpendicular to the vertical plane (assumption of Marston and Anderson [29] which implies unrealistic frictionless interactions within the vertical planes), the value of K_v is equal to the active earth pressure coefficient K_a. The Coulomb assumption $\phi = \phi_c$ leads to a first value of the stress ratio referred to as K_{v1} and deduced from Eq. 6). In practice, the association of the assumption of Roscoe (Eq. 5 and the Eq. 6) leads to a stress ratio $K_{v2} = 1$.

The previous analytical solutions do not take into account the amplitude of the vertical displacement of the trapdoor. Yet, this displacement clearly influences the amplitude of the strains induced in the granular material. Papamichos et al. [32] have proposed a new mechanism analysis to describe the behavior of a granular layer subjected to very minor trapdoor displacements: in this case, the loading, acting on the trapdoor, results from the weight of the granular material located in a cone-shaped failure zone. For a circular trapdoor, this failure zone was assumed to make an angle with the horizontal direction equal to $\pi/4 - \phi/2$.

To investigate the role of the value K and the influence of the trap displacement on the load transfer in the trapdoor problem, an experimental study involving real geomaterials (sand and gravel) is proposed in this paper. Different analytical solutions in the literature are compared with the authors' new experimental results. Moreover, to emphasize the influence of the mechanical characteristics of the granular material on the response of the layer, numerical modeling is carried out by means of the DEM. The DEM is indeed a particularly relevant numerical tool for the modeling of granular material behavior. In addition, the mechanical and physical parameters of this method—similar to real parameters give ample scope for the reproduction of soil properties such as dilatancy, critical state… The numerical results are analyzed at both macroscopic (granular layer) and microscopic scales (grains and contact levels).

2 Experimental study

2.1 Methods

2.1.1 Experimental device

The physical model consisted of a wooden box 1.0 m wide and 0.4 m deep, with a plexiglas front horizontally reinforced with steel bars. Depending on the case studied, the height of the test box ranged from 0.15 to 0.80 m. As shown in Fig. 2, a 0.20 × 0.40 m trapdoor was located in the bottom of the box. The trapdoor was moved downwards incrementally to induce load transfers in the granular layer placed above it. The vertical critical effort, called F, applied by the granular layer on the trapdoor was measured using a load cell with an accuracy of 1 N. In order to limit wall boundary effects on the measurements, the critical effort F was obtained by a load cell in the centered half of the trapdoor (Fig. 2).

The mean pressure p acting on the trapdoor was deduced from F and from the trapdoor dimensions. A test indicator dial gave the trapdoor vertical displacement δ, ranging from 0 to 0.10 m with an accuracy of 0.01 mm. The kinematics of the granular layer was deduced from the displacement of horizontal colored strips of the granular matter using digital image analysis software.

In the trapdoor apparatus, the plane strain conditions were respected and the horizontal stress perpendicular to the plexiglas was not measured.

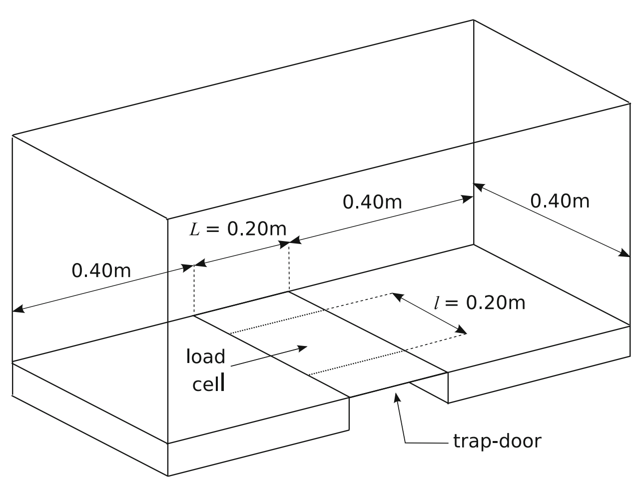

Fig. 2 Diagram of the test box

2.1.2 Characterization of the granular materials

Dry sand and gravel were tested in a loose initial state. The grading and the snapshots of the particles of the two granular materials are given respectively in Figs. 3 and 4. The sand is referred to as S_f and the gravel G_c.

The physical properties of the materials tested are given in Table 1. d_X is the size of the particles in such a way that X percent (in volume) of the grains are smaller than d_X. Consequently, the ratio $C_u = d_{60}/d_{10}$ given in Table 1 quantifies the relative width of the particle size distribution. A value of C_u close to 1 corresponds to a narrow particle size distribution (gravel); inversely, a greater value corresponds to a wide ranged particle size distribution (sand).

The frictional parameters of the different materials were deduced from axisymetric triaxial tests with a constant confining stress σ_r and a constant strain rate $\dot{\varepsilon}_1 \simeq 5 \times 10^{-3}\,\mathrm{s}^{-1}$ in the compression direction. In order to test the samples in similar stress states to those observed in the test box, very low confining stresses were used: 5, 10 and 15 kPa. These confining pressures were obtained with a vacuum pump by applying an equivalent negative pressure (related to atmospheric pressure). To keep a satisfactory ratio between the grain size and the diameter of the tested samples, the materials S_f were tested in a 70 mm diameter test cell, whereas G_c were tested in a 150-mm-diameter test cell.

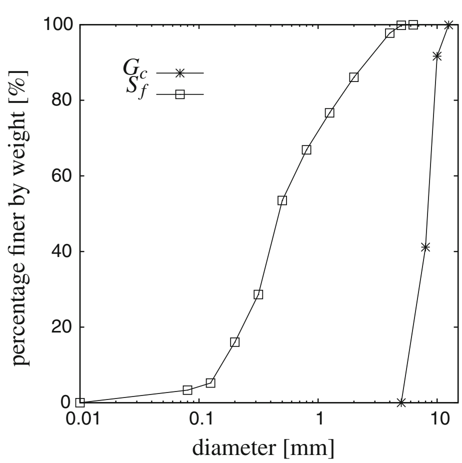

Fig. 3 Grading of the materials

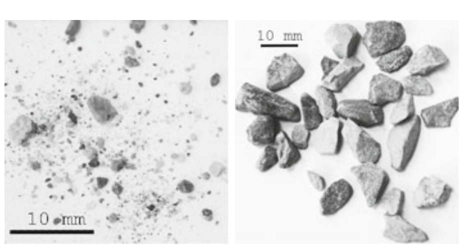

(a) **(b)**

Fig. 4 Snapshots of the materials. **a** S_f. b G_c

Table 1 Physical and mechanical properties of sand and gravel granular materials

			S_f	G_c
Minimal diameter	$d_{\min}$	[mm]	0.01	5.0
Mean diameter	d_{50}	[mm]	0.5	8.0
Maximal diameter	$d_{\max}$	[mm]	6.3	12.5
Uniformity coefficient	C_u	[−]	4.09	1.61
Density	γ_s	[kN/m^3]	26.1	26.5
Apparent density	γ_i	[kN/m^3]	17.0	15.2
Peak friction angle	ϕ_p	[°]	49	54
Critical friction angle	ϕ_c	[°]	39	40

The samples for the triaxial tests were prepared by pouring the granular material into a cylindrical box with no drop height. This classical laboratory procedure enables samples to be obtained with very low solid fraction.

In addition, a correction was applied to the radial confining stress given by the stiffness of the latex membrane surrounding the samples [27]. The effect of the self-weight of the samples was also considered. However, since the self-weight influences the axial stress, its effect on the final value of the measured friction angle was negligible.

From these triaxial tests, two angles of friction can be measured: a peak friction angle ϕ_p corresponding to the maximum strength and a critical friction angle ϕ_c characterizing the mechanical strength for high values of vertical deformation ($\varepsilon_1 \geq 15\%$). These friction angles are shown in Table 1.

The reader is asked to bear in mind that the friction angles are obtained by means of triaxial compression testing in axi-symetry conditions. However, the problem of the trapdoor is a plane strain problem and it is generally accepted that in these conditions, the measured friction angles are greater than in non-plane strain conditions. Thus, the angles given in Table 1 should be considered as minimum values for friction angles.

2.1.3 Trapdoor test procedure

Several 2-cm-thick strata were successively dropped into the test box without compaction in order to form a loose granular layer h thick. The initial apparent density of the material γ_i (Table 1) was equal to its minimal density. The layer thickness ranged between 0.05 and 0.60 m. The pressure acting on the trapdoor during the filling process of the test box was compared with the theoretical value $\gamma_i\, h$: a gap less than 2 % was observed between the measured and expected values.

The total trapdoor displacement was referred to as δ. The trapdoor was moved at a rate of 1.0 mm per min. and stopped for several positions corresponding to different values of δ: every 0.1 mm increment for $0 \leq \delta \leq 5$ mm, then every 0.5 mm increment for $5 \leq \delta \leq 25$ mm and finally every 1.0 mm increment for $\delta \geq 25$ mm. Due to this test procedure, the problem was considered to correspond to quasi-static conditions.

The portion of granular material located under the bottom of the test box and above the trapdoor (Fig. 5) did not participate in the load transfer but contributed to the increase of p when the trapdoor moved downwards. It is then advisable to use the variable q corresponding to the mean pressure acting at the initial position of the trapdoor (at the bottom of the test box). Assuming that the load transfer between the granular material and the walls around the trapdoor tends to zero, the value of q can be written

$$q = p - \gamma_i \delta \tag{10}$$

assuming that the density of the granular material under the bottom of the test box is equal to the initial apparent density.

2.2 Results

The load responses obtained with each granular material and for each layer h thick broke down into three characteristic phases that corresponded to precise conditions with regard to kinematics and to load transfer amplitudes. A typical response is given in Fig. 6 and showing p versus δ for a 0.20-m-thick layer of G_c. The granular layer response for this test consisted in

(i) phase (a): a phase of maximal load transfer during which the pressure reached a minimum value $p_{\min}$. This phase occurred as soon as the trapdoor was moved downwards from its initial position $0.3 \leq \delta \leq 4.5$ mm, depending on the granular material tested,

(ii) phase (b): a transitional phase during which the pressure p increased with δ (the increase rate of p with δ was constant for all tests for a given material),

(iii) phase (c): a critical phase during which two vertical shear bands were observed starting at each edge of the trapdoor. During this phase, the pressure p increased continuously with δ but at a reduced rate. The first observation of the vertical shear band gave the critical pressure notes p_c.

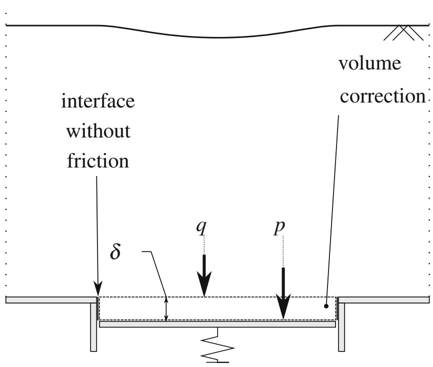

Fig. 5 Definition of the pressure q acting on the trapdoor depending on the volume of the material located under the *bottom* of the test box and not participating in the load transfer

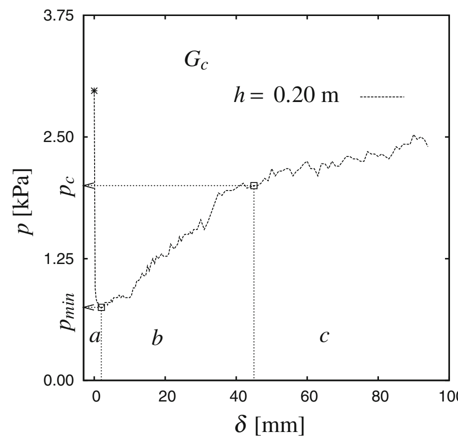

Fig. 6 Description of the three successive phases of the trapdoor problem (case G_c, $h = 0.20$ m): (a) maximal load transfer, (b) transitional phase, (c) critical phase

Figure 7 shows load transfer p obtained with various layer thicknesses for materials S_f and G_c.

2.2.1 *Phase (a): Maximum transfer phase*

The maximal load transfer phase, referred to as phase (a), corresponded to the minimal pressure $p_{\min}$ measured on the trapdoor or to the minimal corrected pressure $q_{\min}$ on the trapdoor.

As shown in Fig. 7, minimal pressure was reached for a very small displacement of the trapdoor. Figure 8 shows the displacement δ required to reach $p_{\min}$ versus the height of the granular layer for both materials. Phase (a) was obtained for lower values of δ in the case of S_f than in the case of G_c. The mechanism observed in the trapdoor problem corresponds to the mobilization of the friction on the interfaces between the soil above the trapdoor and the material on either side. Thus, the relative displacement between both parts required to fully mobilize the friction on these interfaces was greater for G_c, which presented a larger particle size.

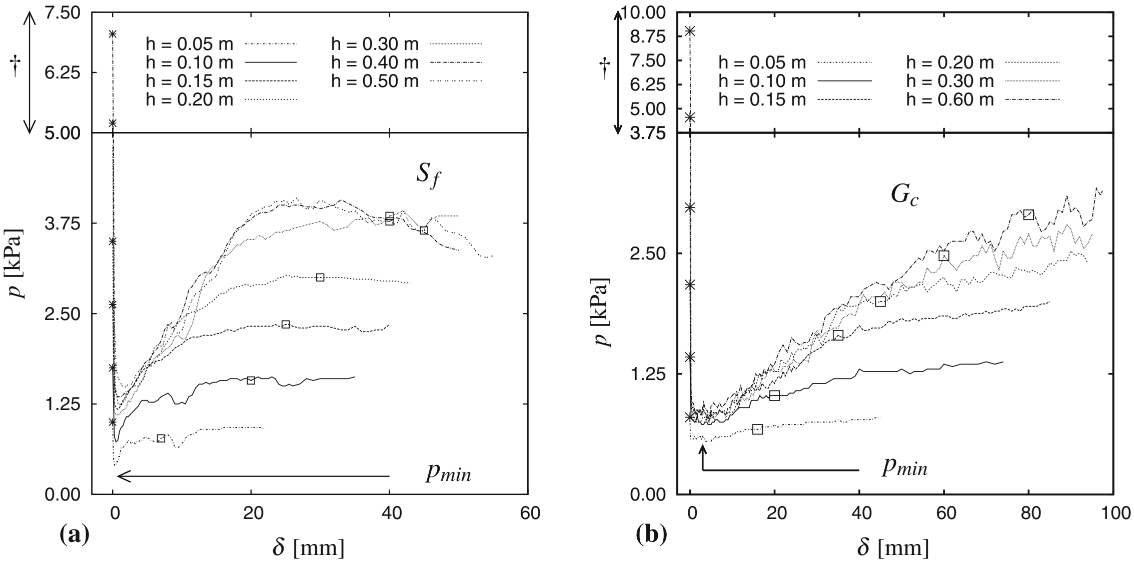

Fig. 7 p versus δ for S_f and G_c and for various layer thicknesses h; the *square* symbols correspond to the first observation of vertical shear banding (the symbol *dagger* underlines a change in the scale of the y axis). **a** Sand. **b** Gravel

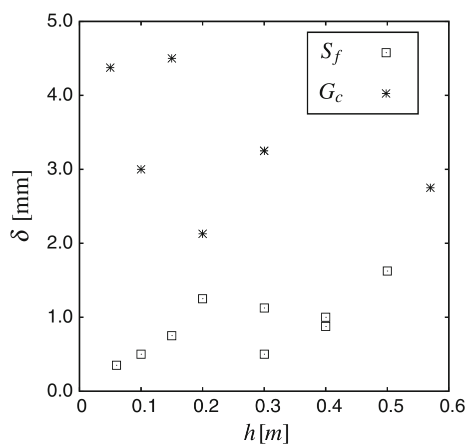

Fig. 8 Trapdoor displacement δ necessary to reach maximal load transfer, corresponding to minimal pressure

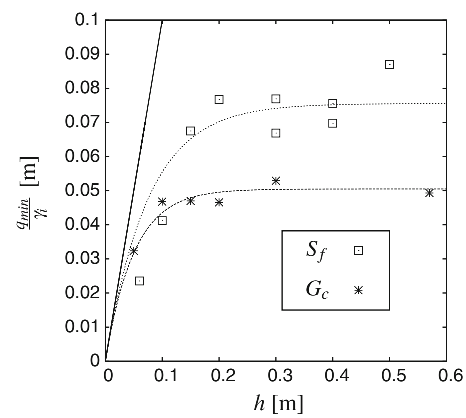

Fig. 9 $q_{\min}/\gamma_i$ versus h for S_f and G_c. The *line* corresponds to the values predicted by the Eq. 1 using the angle of friction ϕ_p of each granular material and the following stress ratio: $K = 1.17$ for S_f and $K = 1.46$ for Gravel

Figure 9 shows the relation between the weighted minimal pressure $q_{\min}/\gamma_i$ and the thickness of the layer for S_f and G_c. Without any load transfer, a granular layer of thickness h and volumetric weight γ_i would apply a pressure equal to $q_{\min} = h\gamma_i$ on the trapdoor which corresponds to the solid line of slope 1:1 in Fig. 9. The experimental results showed that $q_{\min}/\gamma_i$ reached a threshold as the thickness of the layer exceeded a specific value h^*, which depended on the material:

- for S_f: $q_{\min}/\gamma_i \simeq 0.08$ for $h > h^* = 0.10$m,
- for G_c: $q_{\min}/\gamma_i \simeq 0.05$ for $h > h^* = 0.15$m.

The relation of minimal pressure with h was computed using Eq. 1 in which a coefficient K and a friction angle ϕ are needed. The friction angle ϕ_p is strongly correlated with the initial state of the granular layer and is obtained for a level of minor strain. Due to the small displacement level involved in phase (a), the peak friction angle ϕ_p was chosen. The dashed lines in Fig. 9 shows that Eq. 1, obtained by adjusting K, is an acceptably close fit to the experimental values.

$$K = \begin{cases} 1.17 \pm 0.06, & \text{for } S_f \\ 1.46 \pm 0.03, & \text{for } G_c \end{cases}. \tag{11}$$

Briefly presented in Sect. 1, most of the analytical solutions involving a coefficient K related to the value of the friction angle ϕ of the granular material. Due to the assumed kinematics along the vertical planes, K is often assumed to correspond to the active earth pressure coefficient K_a [29, 30] taking values always lower than 1.0. However, the values of K resulting from the fit were greater than 1.0. Consequently, for phase (a), K could not correspond to the active earth pressure coefficient.

Furthermore, the reliance of K on ϕ for phase (a) represented a real problem and other effects might influence the behavior of the granular layers for phase (a): material grading, ratio of mean particle size to trapdoor size, initial relative density of the granular soil. The experimental study involved natural geomaterials which presented numerous differences as far as physical parameters were concerned such as grain shape, surface properties. An attempt to highlight the influence of the friction angle ϕ and grain shape with the DEM is proposed in Sect. 3.

2.2.2 Phase (b): The transitional phase

The transition phase between the maximal load transfer phase and the critical phase corresponded to the increase of p and q with δ. During this phase, the soil above the trapdoor progressively expanded as the trapdoor moved downwards. The weight of granular material supported by the trapdoor increased. An expansive zone delimited by two inclined planes starting at each edge of the trapdoor was observed in Figs. 10 and 11. At the end of the transitional phase, these planes were vertical. Two parameters characterized phase (b): the interval of displacement "δ-range" necessary to make the transition and the gradient $k = \mathrm{d}q/\mathrm{d}\delta$.

In Fig. 12, it can be observed that the interval δ-range of phase (b) increased with the thickness h of the layer and was greater for G_c than for S_f. The values of the pressure q versus δ corresponding to phase (b) are shown in Fig. 13 for materials S_f and G_c. For a given material, the gradient of q with δ during the transitional phase was independent of h if $h \geq h^*$. For each material, once h is greater than h^*, a linear regression of the experimental measurements gave the values of gradient k:

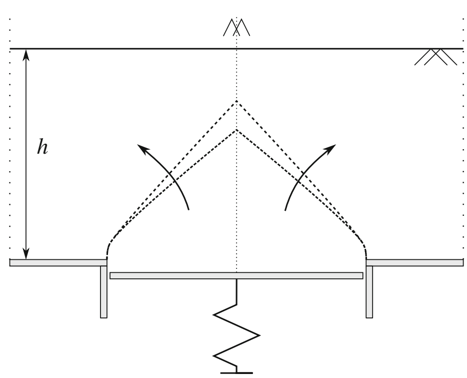

Fig. 10 Transitional phase: expansion zone

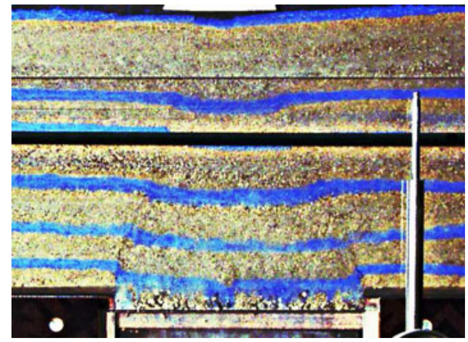

Fig. 11 Snapshot of the expansion zone during transitional phase (case of S_f, $h = 0.20$ m, $\delta = 10$ mm)

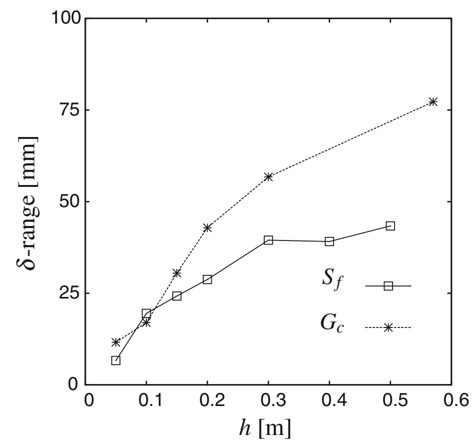

Fig. 12 δ-range during which the transitional phase occurs versus the layer thickness h for S_f and G_c

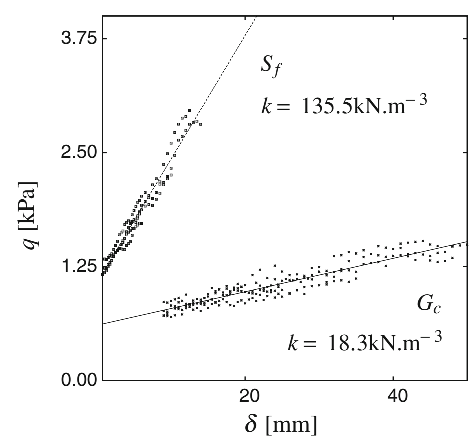

Fig. 13 Corrected pressure q versus δ for phase (b) for S_f and G_c and for $h \geq h^*$

$$k = \begin{cases} 135.5 \pm 2.6\,k\mathrm{N\,m^{-3}}, & \text{for } S_f \\ 18.3 \pm 0.5\,k\mathrm{N\,m^{-3}}, & \text{for } G_c \end{cases}. \tag{12}$$

The value of k represents the ability of the granular material to maintain the load transfers obtained at the end of phase (a): the high values of k mean that the load transfers decrease rapidly, whereas the low values of k correspond to a good conservation of load transfers. The difference between the values of k for S_f and G_c showed that the gravel was much more able to transfer the load from the expansion zone to the remaining parts of the layer.

An estimation of the intensity of load transfers during phase (b) was made: the volumes of expansion zones were deduced from image analysis. The pressure q_w induced by this volume on the trapdoor was calculated as if no load transfer existed between the expansion zone and the remaining material. To do so, the surface s of the vertical cross section of the expansion zone was deduced from image analysis. The resulting weight of the expansion zone was then calculated based on a material density equal to γ_i. The resulting expression of q_w is:

$$q_w = \gamma_i \left(\frac{s}{2B} - \delta \right) \tag{13}$$

where $2B$ is the trapdoor width, γ_i the initial apparent density and s the area of the expansion zone in a vertical cross section of the test box (Fig. 14). Figures 15 and 16 show the comparison of data (δ, q_w) and (δ, q).

A new gradient k_w was calculated from the data (δ, q_w), this gradient corresponded to a response without load transfer. For G_c, the analysis of two trapdoor tests gave a mean value $k_w(G_c) = 56.7$ kN m^{-3}. For S_f, the analysis of four tests gave a mean value $k_w(S_f) = 147 \pm 60$ kN m^{-3}. The comparison of the increase rates k and k_w confirmed the difference in behavior of the two materials tested for the transitional phase:

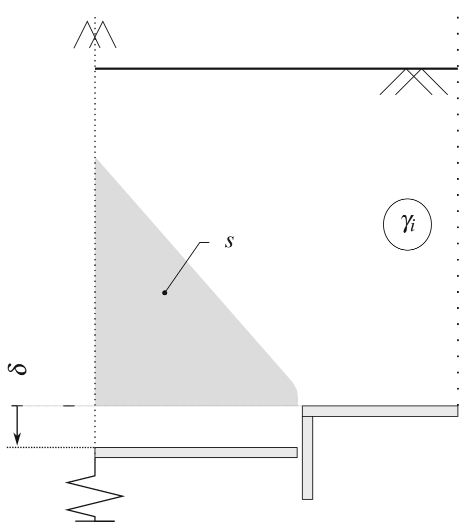

Fig. 14 Area s of the expansion zone in a vertical cross section of the test box

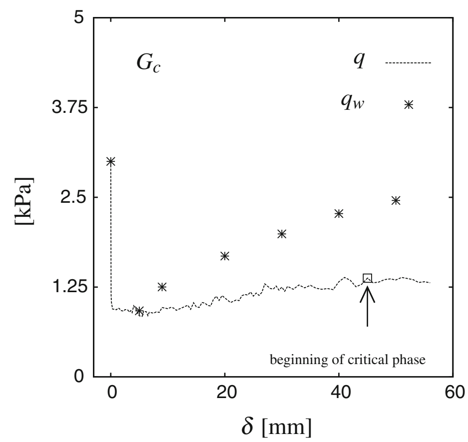

Fig. 15 Comparison of q and q_w versus δ for G_c and $h = 0.20$ m

$$\begin{cases} k_w/k = 1.10 \pm 0.45 & \text{for } S_f \\ k_w/k = 3.05 \pm 0.45 & \text{for } G_c \end{cases}. \tag{14}$$

A ratio $k_w/k \approx 1$ means that no load transfer exist between the expansion zone and the remaining material, whereas a ratio $k_w/k \geq 1$ means that load transfers exist. Basically, $k_w/k < 1$ is not physically correct. Assumptions made for the computation might explain the inconsistency of some results: the failure zone observed through the front plexiglass wall was assumed to be representative of the whole layer. For S_f, the ratio k_w/k was centered on a value of 1.10, which corresponds to a quasi no load transfer mechanism from the expansion zone to the remaining material. For G_c, the ratio was about 2.6: the gravel was thus much more able to mobilize friction at the interfaces than the sand.

2.2.3 *Phase (c): The critical phase*

During the critical phase, the whole column of soil over the trapdoor was involved in the sliding movement, contrary to previous phases. Phase (c) corresponded to the classical description of the trapdoor problem with a considerable displacement: two vertical planes, starting at each edge of the trapdoor, marked the boundaries between a volume of granular material sliding between two fixed parts (Figs. 17 and 18). The pressure p_c on the trapdoor for the critical phase was measured at the beginning of the phase, i.e. as soon as the boundaries of the slipping zone became vertical.

During phase (c), the surface of the layer settled because of the substantial displacements involved. Consequently, a corrective value h' of the height h of the granular layer was defined (Fig. 19). The evolution of q_c according to h' given in Fig. 20 showed that there was a value of $h' = 0.27$m for

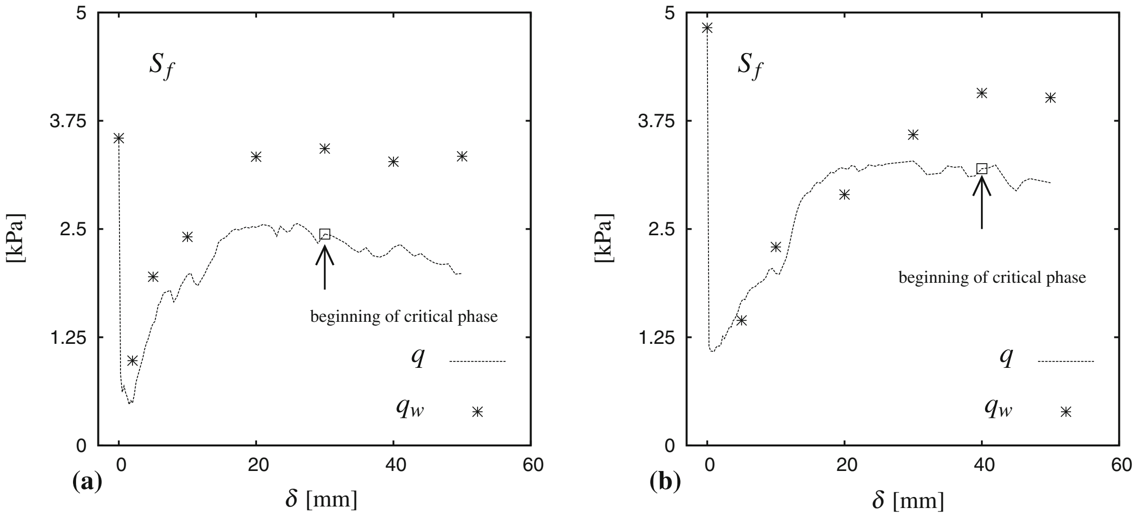

Fig. 16 Comparison of q and q_w versus δ for S_f. **a** h = 0.20 m, **b** h = 0.30 m

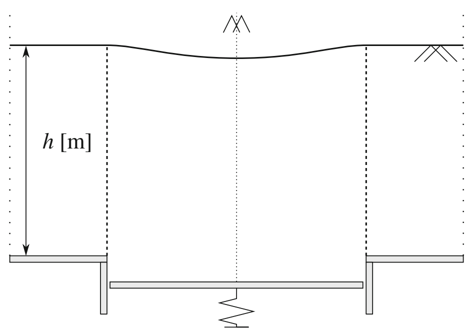

Fig. 17 Critical phase: vertical boundaries of the sliding zone of the granular layer

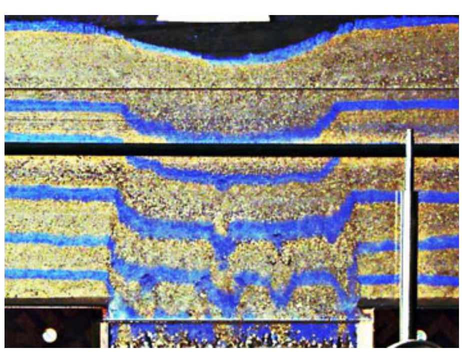

Fig. 18 Snapshot of the granular layer during critical phase (case of S_f, $h = 0.20$ m et $\delta = 40$ mm)

which q_c reached a maximum. For G_c, q_c reached a threshold.

Once again, phase (c) was associated with considerable deformations. It seemed fairly intuitive to accept that the shear strength of the material to be considered corresponded to the critical friction ϕ_c. Despite very close

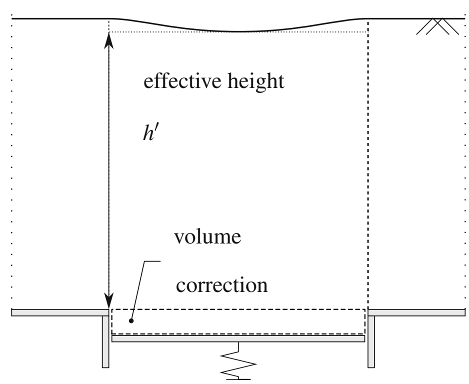

Fig. 19 Corrections for critical phase on the effective height of the granular layer

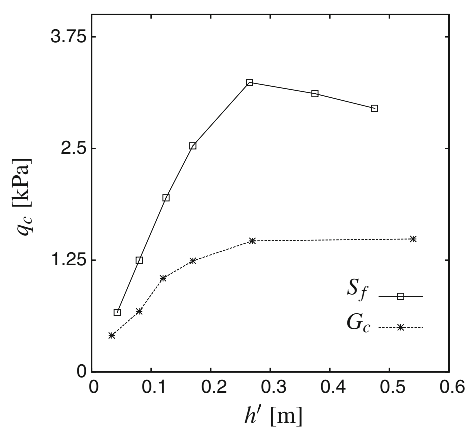

Fig. 20 Critical pressure q_c versus h' for S_f and G_c

values of critical friction angles for both materials – $\phi_c = 39°$ for S_f and $\phi_c = 40°$ for G_c—the critical pressures q_c were approximately twice as great for S_f as for G_c.

The results obtained for phase (c) were compared with the predictions of the analytical solution of Eq. 1. Since the analytical solution does not consider the vertical displacement of the trapdoor δ, the value of the prediction was assumed to be equal to the equivalent pressure at the level of the bottom of the test box.

$$q_c(h') = \frac{B\gamma}{K \tan \phi_c}\left(1 - e^{(-Kh'/B)\tan\phi_c}\right) \tag{15}$$

where $2B = 0.20$ m is the width of the trapdoor, ϕ_c the critical friction angle along the vertical failure planes, h' is the effective height of the layer and K a coefficient corresponding to the ratio between the horizontal and the vertical stresses. The volumetric weight γ used here was the initial volumetric weight of the granular layer γ_i.

The analytical solutions were compared with the experimental results for phase (c). The coefficients K given

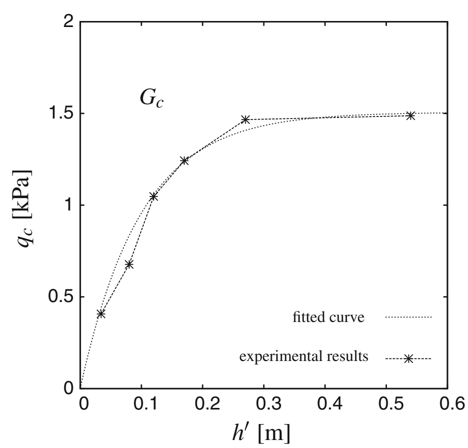

Fig. 21 Comparison between the experimental results and the analytical description of Eq. 15 leading to a coefficient $\{K\}_{fit} = 1.19 \pm 0.04$

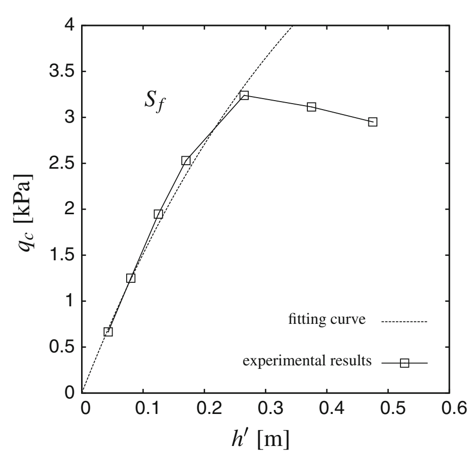

Fig. 22 Comparison between the experimental results and the analytical description of Eq. 15 leading to a coefficient $\{K\}_{fit} = 0.30 \pm 0.03$

by the different analytical solutions were compared with the coefficient $\{K\}_{fit}$ able to fit the experimental data with respect to Eq. 15. For the gravel G_c, the shape of the experimental curve giving q_c versus h' reproduced the Eq. 15 with $K = 1.19 \pm 0.04$ well (Fig. 21).

For the sand S_f, the experimental curve giving q_c versus h' broke down into two parts separated by a break of slope for $h' = 0.27$m. This shape could not be efficiently reproduced by Eq. 15 (Fig. 22). A minimal value of K could be obtained by fitting the first part of the curve. The values of the coefficient K given by the analytical model and by the approximation to the experimental data are given in Table 2.

For G_c, the value of $\{K\}_{\text{fit}} = 1.19$ required to fit the experimental data was greater than any proposition of the analytical models. Moreover, this result showed that horizontal stress should be greater than vertical stress: the soil was under extension conditions.

For S_f, the fitting of the experimental data with the Eq. 15 for $h' \leq 0.30$ gave a coefficient $\{K\}_{\text{fit}} = 0.30$, which was not very far from the coefficient proposed by Marston and Anderson. However, the break of slope obtained could not be analytically obtained. The decrease in critical pressure p_c as h increased was in contradiction with the results obtained with the gravel but also with all the analytical solutions. The solutions predicted indeed that a threshold convergence of the pressure should be reached but not a decrease. Consequently, the last experimental points should be considered carefully. Some experimental artefacts might have disturbed the response of the sand layers for high thickness values and high values of trapdoor displacements.

2.2.4 *Synthesis of the experimental part of the study*

A systematic break down of the responses of the granular layers into 3 phases was observed. These phases showed that the load transfers in the granular layers were directly correlated with the value of the trapdoor displacements. The maximal load transfer amplitude was observed at the beginning of the trapdoor movement.

Table 2 Coefficient K predicted by some analytical models based on Eq. 15

	S_f	G_c
Marston and Anderson	0.23	0.23
Handy	0.40	0.38
Coulomb	0.44	0.43
Roscoe	1.00	1.00
Fit	0.30 ± 0.03	1.19 ± 0.04

The minimal pressure $q_{\min}$ on the trapdoor increased with the granular layer thickness h as long as $h < h^*$ and then reached a threshold for $h > h^*$, with $h^* = 0.15$ m for the sand S_f and $h^* = 0.10$ m for the gravel G_c. The evolution of $q_{\min}$ with h was reproduced successfully by the solution of Eq. 15. The analytical modeling of $q_{\min}$ highlighted the importance of the stress ratio K. For both granular soils, K was greater than 1.0 so the horizontal stresses were bigger than the vertical ones. As soon as $h > 0.1$ m, it was observed that transfers were higher for gravel than for sand. Moreover, the amplitude of trapdoor displacement $\delta_{\min}$ corresponding to $q_{\min}$ was higher for G_c than for S_f, indicating that a correlation might exist between $\delta_{\min}$ and the grain size.

The load transfers initially developed during the first phase gradually decreased during the second phase. The increase of the pressure on the trapdoor, due to the progressive loosening of the soil over the trapdoor, evolved linearly as the trapdoor was moved downwards. The gradient $\mathrm{d}q/\mathrm{d}\delta$ was constant for a given material: this gradient—which depends on the interaction between the unpacked soil and the adjacent areas—showed the ability of the granular material to maintain the load transfer initially developed. This ability was obviously greater for G_c than for S_f. From a kinematics point of view, this phase was associated with an expansion of the failure zone from the bottom of the layer to its surface.

Finally, for considerable displacements of the trapdoor, the pressure on the trapdoor reached a threshold in most cases, depending on the thickness of the layer. Two tests on sand showed a drop in pressure for extensive displacement of the trapdoor: it occurred for a substantial height of the granular layer; therefore, a "silo effect" with walls might have modified the testing conditions. The behavior during phase (c) corresponded to the sliding of the material located above the trapdoor between two vertical failure planes. The pressure on the trapdoor could be modeled by the equation of Janssen Eq. 15 by an adjustment of the stress ratio K. This modeling was particularly satisfying in the case of the gravel layers. Many analytical expressions of the stress ratio K were calculated and compared with those obtained by fitting with the experimental data. For sand, the coefficient K was consistent with the range of analytical values. For gravel, K was greater than 1.0 which is consistent with the situation in which a granular layer is subjected to a vertical extension.

In order to clarify these observations, a set of very well-controlled materials were needed and consequently, a numerical modeling of the trapdoor problem involving the DEM was carried out.

3 Numerical study

The DEM is a useful and relevant numerical tool for the modeling of granular materials such as those dealt with in the first part of this paper. The full control of parameters such as particle shape, grading and macro-mechanical parameters is a means of answering the questions raised previously.

3.1 Methods

3.1.1 The discrete element method (DEM)

The principle of the DEM is to model granular materials with non-deformable particles that interact with each other through contact points. While the *Contact Dynamics* method [31] governs contact behavior in Signorini conditions (rigid contact), the *Molecular Dynamics* approach used here takes into consideration contact elasticity [17]. The kinematics of the media is governed by the equations of motion applied to each particle:

$$M\ddot{\mathbf{x}}_i = \sum_j \mathbf{F}^{j\to i} + \mathbf{r} \tag{16}$$

$$\underline{\underline{I}}\ddot{\Theta}_i = \sum_j \Gamma^{j\to i} + \mathbf{m}_r \tag{17}$$

where:

- M is the mass of particle i and $\underline{\underline{I}}$ its matrix of inertia,
- $\ddot{\mathbf{x}}_i$ is the translation acceleration of i and $\ddot{\Theta}_i$ its angular acceleration,
- $\mathbf{F}^{j\to i}$ is the force applied by particle j on i, $\Gamma^{j\to i}$ is the moment induced by $\mathbf{F}^{j\to i}$,
- $\mathbf{r}$ represents the action on i of external forces and $\mathbf{m}_r$ the moment induced by $\mathbf{r}$ on the center of gravity of i.

The double integration of the equations of motion is carried out according to an explicit *Verlet* numerical scheme [3]. In addition, a local damping coefficient is used at each time-step to reduce the unbalanced forces acting on the particles. A new term is added to Newton's second law of motion because of this damping [18]. This damping method influences acceleration values and is expressed through a non-dimensional parameter α. In the modeling presented in this paper, the damping coefficient was set at $\alpha = 0.75$. Since the numerical study consisted of successive equilibrium states, the damping method did nothing more than enable a stable mechanical state to be reached rapidly. There was no influence of α on the results observed.

At each contact point, normal and tangential components of the contact force are governed by linear contact laws. The normal component of the contact force applied by particle j on particle i can be written as follows

$$f_n^{j \to i} = K_n h^{ij} \tag{18}$$

where K_n represents the normal contact stiffness and h_{ij} the overlap of the two particles i and j with $h_{ij} > 0$ for the overlapped particles. No traction was considered here between particles. The tangential component of the contact force $\mathbf{f}_t^{j \to i}$ is linked to the relative tangential incremental displacement δu_t of particles i and j with a stiffness K_t [17] by the following expression

$$\frac{\mathrm{d}\left\|\mathbf{f}_t^{j \to i}\right\|}{\mathrm{d}\delta u_t} = K_t \tag{19}$$

and is bound by a Coulomb friction criterion

$$\|\mathbf{f}_t^{j \to i}\| \leq \mu f_n^{j \to i} \tag{20}$$

with μ the contact friction coefficient between particles i and j.

The code used was SDEC software [20] developed in the 3S-R laboratory, which is based on 3D molecular dynamics.

3.1.2 Granular model

Two kinds of particles were used (Fig. 23):

- spherical particles,
- complex particles, referred to as clusters.

A cluster is a perfectly rigid assembly of two overlapped, identical spheres of diameter d. Two different values of the distance between the centers of spheres of the cluster were modeled: 0.20d and 0.95d. Finally, three particle shapes were then modeled: spheres (S), clusters with a distance between the centers of spheres of, 0.20d (C^{20}) and clusters with a distance between the centers of spheres of, 0.95d (C^{95}).

The concavity of cluster particles implies that two of the latter may be in contact through more than one contact point. In addition, simple spheres can roll without slipping on each other, this phenomenon is no longer valid in the case of cluster particles due to the concavity and the increased interweaving of the particles. Consequently, using clusters introduces a geometrical resistance to this rolling, and the range of shear strength attainable with such assemblies is much greater than that for spherical particles [11, 36, 38, 39]. Friction angles as high as those found with the geomaterials used in the experimental study were thus modeled.

The grading of the modeled particle assemblies (Fig. 24) was characterized by a ratio of the maximal diameter to the minimal diameter

$$\frac{d_{\max}}{d_{\min}} = 2.66 \tag{21}$$

Within this range of diameter, particle sizes were randomly chosen in such a way that the coefficient of uniformity of the assemblies was equal to $C_u = 1.52$. In the experimental study, the gravel G_c presented a uniformity coefficient of, $C_u = 1.61$ (Table 1).

3.1.3 Numerical parameters and mechanical properties

The aim of the numerical study was to investigate the influence of the macro-mechanical parameters of a granular material on its response to the trapdoor problem. Load transfers in granular materials are closely linked to shear strength and particularly to friction angles in both peak and critical states. Consequently, several granular assemblies with various macro-mechanical parameters were modeled.

The macro-mechanical parameters of an assembly of particles depend on:

- physical parameters such as porosity, grading [10], particle shapes [11, 36, 38, 39],
- mechanical parameters of contact laws such as stiffnesses and friction coefficient in the case presented in this paper [2, 6, 14, 35],

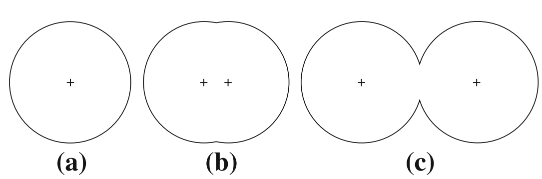

Fig. 23 Particle types: **a** spherical, **b** cluster 0.20d, **c** cluster 0.95d

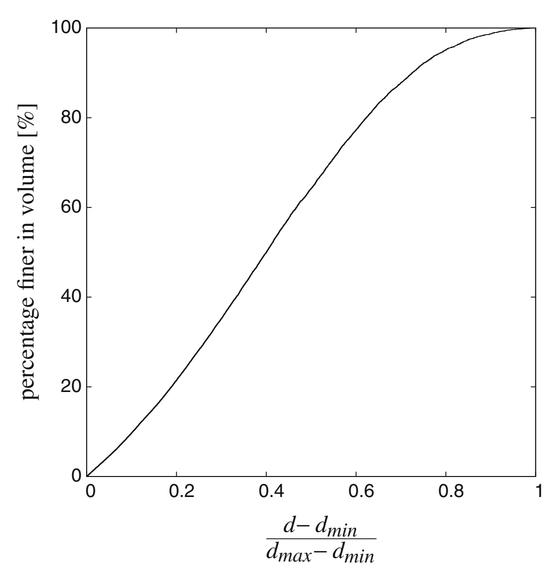

Fig. 24 Grading of numerical particle assemblies

- the way used to prepare granular assemblies [4, 5, 9, 16]

The mechanical characterization of each type of assembly was carried out by modeling triaxial tests on samples of 8000 particles with a constant confining stress $\sigma_3 = 5$ kPa.

To set contact stiffness, rigidity κ of the granular assembly was used. The parameter κ [15] is a non-dimensional parameter used to quantify contact deformability. It is related to the mean overlap $\langle h \rangle$ of particles in an assembly. With this parameter, the stiffnesses of the experimental and numerical samples can be compared. For a linear normal contact law in 3 dimensions, κ is defined by

$$\kappa = \frac{\langle K_n \rangle}{\langle d_r \rangle P} = \frac{\langle d_r \rangle}{\langle h \rangle} \tag{22}$$

where $\langle K_n \rangle$ is the mean normal stiffness of the contacts, P is the equivalent isotropic pressure on the assembly and $\langle d_r \rangle$ is the mean diameter of the particles. The stiffness level of the sample modeled in this study was equal to $\kappa = 3{,}125$. This value presents the same order of magnitude as for monodisperse glass beads submitted to an isotropic pressure of 100 kPa. For tangential stiffness K_t, Schäfer et al. [37] and Combe [13] showed that a value of K_t/K_n between 0.5 and 1 has no significant influence on the simulated mechanical behavior. Emeriault et al. [22] showed that $K_t/K_n \geq 1$ could lead to assemblies with negative Poisson ratios. Consequently, the ratio K_t/K_n was fixed at 0.75.

For the triaxial tests, numerical samples were generated using Radius Expansion with the Decrease of Friction process (REDF) [9]. Particle diameters were progressively increased until an isotropic pressure threshold $P_{max} = 500$ Pa was reached on the walls. After that, the porosity η of the assembly was assumed to be maximal $\eta = \eta_{max}$. As the isotropic pressure could not be lowered below the threshold value, the contact friction coefficient μ was progressively reduced so that particle expansion could proceed until the contact friction coefficient reached the value of $\mu = 0$. The porosity was then minimal, $\eta = \eta_{min}$. With this generation method, the assembly could be generated with any desired value of porosity within the range $[\eta_{min}, \eta_{max}]$. The porosities of the different assemblies are summarized in Table 3.

Assemblies of different particle shapes and porosities were set up in order to obtain an extensive range of macroscopic peak and critical friction angles: $\phi_p \in [24.5°, 49°]$ for the peak friction angle and $\phi_c \in [21.7°, 31.3°]$ for the critical friction angle. Each particle shape gave a unique value of the critical friction angle. For samples of particles S and C^{20}, only the initial porosity of the sample was modified. For samples of particles C^{95}, only the contact friction coefficient was modified. In order to focus on the effect of the particle shape, the ranges of peak friction angle associated with each shape have to overlap each other. The value of friction coefficient had to be unique for almost all cases. These two conditions led to choose a value of friction coefficient $\mu = 1.466$ (Table 3).

The responses of the samples giving the ratio $(\sigma_1 - \sigma_3)/(\sigma_1 + 2\sigma_3)$ (with σ_1 the axial stress) and the volumetric strain ε_v versus axial strain ε_1 are given in Fig. 25. The mechanical properties of all the assemblies are summarized in Table 3.

Table 3 Physical and mechanical properties of particle assemblies

Shape	S_1 ←	S_2 spherical	S_3 →	C_1^{20} cluster 0.20d	C_2^{20}	C_1^{95} cluster 0.95d	C_2^{95}
η (−)	0.401	0.379	0.355	0.354	0.300	0.405	
η_{min} (−)	0.347	0.347	0.347	0.295		0.347	
η_{max} (−)	0.402	0.402	0.402	0.394		0.444	
μ (−)	1.466	1.466	1.466	1.466		0.521	1.466
E (MPa)	3.39	5.79	7.25	7.09	13.78	4.95	5.88
ϕ_p (°)	24.5	30.7	37.1	37.2	49.0	35.2	46.2
ϕ_c (°)	21.7	22.4	22.2	24.6	24.5	31.3	31.3

3.2 Test procedure and granular layers

3.2.1 *Test procedure*

The assemblies of particles were placed in a test box presenting the same geometry as the experimental device in x and z-axis directions (Fig. 26). In the y-axis direction, the test box width was equal to 0.10 m. The thickness of every layer tested here was equal to $h = 0.20$ m. The number of particles was equal to $N = 23{,}000$. The granular assemblies were prepared in this test box without any gravity by using the REDF procedure [9]. After generation of the assembly, gravity forces were applied to the sample. As for experimental tests, the trapdoor was moved downwards at a constant rate and stopped every 1.0 mm increments for pressure measurements. For each increment, an equilibrium state was reached with the following criterion:

$$\left| 1 - \frac{F_z}{W} \right| \leq 10^{-3} \tag{23}$$

where F_z represents the vertical resultant force applied by the sample on the test box and W is the total weight of the granular layer.

3.2.2 *Initial state*

Before moving the trapdoor, the initial states were checked with regard to distribution of the horizontal and vertical stresses in the sample, orientation of the contacts and

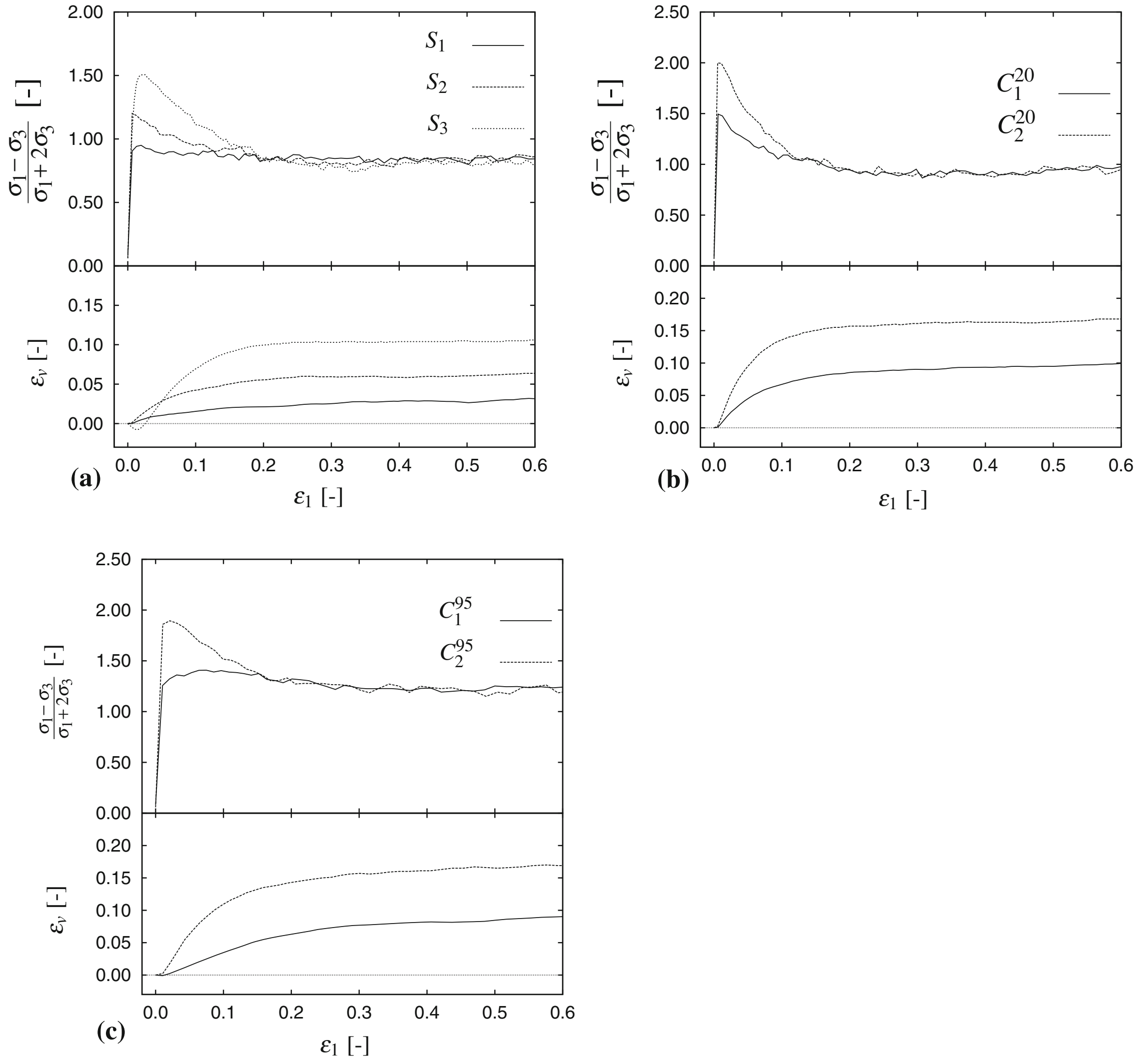

Fig. 25 Responses of the samples to the triaxial test. **a** Spheres. **b** Clusters 0.20*d*. **c** Clusters 0.95*d*

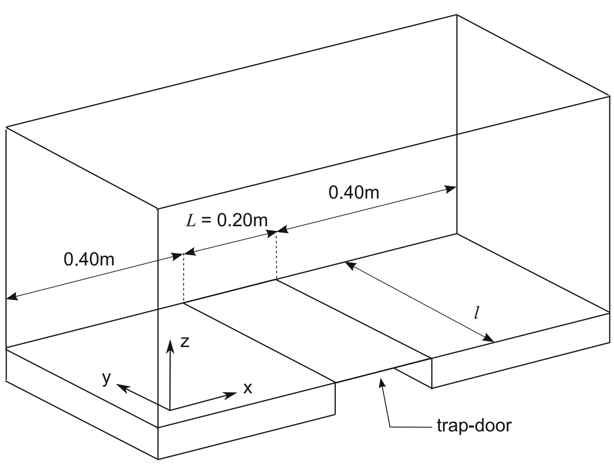

Fig. 26 Diagram of the modeled test box

homogeneity of the porosity. The characterization of the initial state is presented here for sample C_1^{20}.

Figure 27 gives the distribution of the vertical and horizontal stress versus the depth of the granular layer. In a volume V, the stress tensor was calculated by

$$\sigma_{ij} = \frac{1}{V}\sum_{\alpha=1}^{N_c} f_\alpha^i l_\alpha^j \tag{24}$$

where N_c is the number of contact points in V, f^i the projection of the contact force $\mathbf{f}$ on i-axis and l^j the projection of the branch vector $\mathbf{l}$ on j-axis with $i = x, y, z$ and $j = x, y, z$ [46]. The branch vector $\mathbf{l}$ is defined by the vector linking the centers of particle masses in contact. The volume V consisted of horizontal slices of the layer, each one 0.025 m thick.

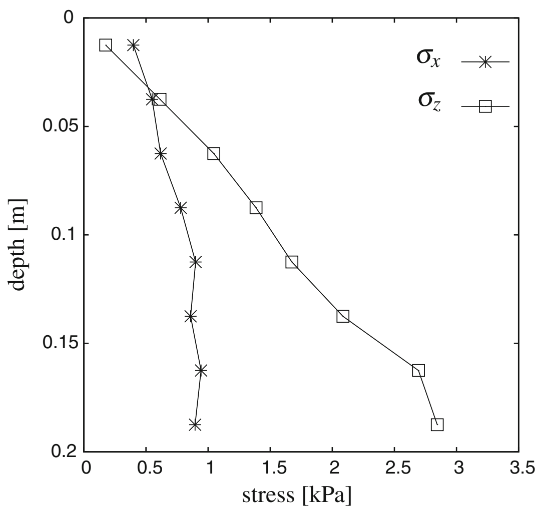

Fig. 27 Distribution of horizontal and vertical stresses σ_x and σ_z versus the depth in the layer for the C_1^{20} sample

As expected, Fig. 27 shows a depth-proportional distribution of the vertical and horizontal stresses, σ_x and σ_z. In addition, the ratio between σ_x and σ_z was constant and around $\sigma_x/\sigma_z \approx 0.4$, except at or near the top of the layer, where the stress state was expected to be isotropic (fluid zone) [21].

The orientations of the contacts with respect to the z-axis direction were computed. The angle θ between the normal to contact plane and the z-axis direction was calculated. The distribution of $|\cos\theta|$, referred to as $P(\cos\theta)$ can be decomposed with Legendre polynomials [21]. According to this decomposition, an isotropic distribution of contacts corresponds to $\frac{1}{N_c}\sum_{N_c}\cos^2\theta = 1/3$ and $\frac{1}{N_c}\sum_{N_c}\cos^4\theta = 1/5$.

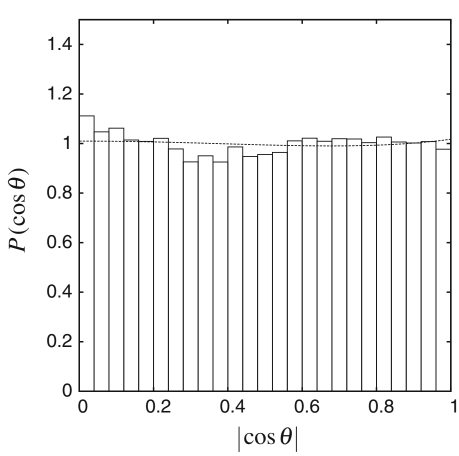

Fig. 28 Distribution of the orientation of contacts $P(\cos\theta)$ with a *vertical direction* in the central part of the sample C_1^{20} in the initial state

The statistical distribution of the orientation of the contacts $P(\cos\theta)$ is given in Fig. 28 for sample C_1^{20}. Only the central part of the sample was considered in this distribution, in order to deactivate the effect of the walls. The initial state was very close to an isotropic state. In this example, $\frac{1}{N_c}\sum_{N_c}\cos^2\theta = 0.3328$ and $\frac{1}{N_c}\sum_{N_c}\cos^4\theta = 0.2001$ were obtained. These values are very close to those expected in isotropic conditions.

3.3 Trapdoor tests: 3 phases

The responses to the trapdoor test of all the samples are shown in Fig. 29 in terms of pressure p and corrected pressure q on the trapdoor, versus trapdoor displacement δ. As with the experimental tests, three phases were observed in the response of the materials to the trapdoor test. The boundary of each phase is more precisely shown for material C_1^{95} on the curve giving corrected pressure q versus δ in Fig. 30.

Figure 31 shows the displacement fields in the vertical cross section of the layer which was analyzed for different values of δ, corresponding to the different phases observed experimentally. A good qualitative and quantitative agreement existed between the numerical modeling using the DEM and experimental testing. The three phases were underlined in this section for sample C_1^{95}.

3.3.1 Phase (a)

As in the experimental tests, the mean pressure on the trapdoor decreased from the initial value to a minimal value $q_{\min}$ as soon as the trapdoor was moved (Fig. 30—part a). At the same time, a wedge-shaped zone located above the trapdoor appeared on the displacement field (Fig. 31a) while the remaining part of the layer was not affected by trapdoor displacement.

The experimental results in Fig. 9 show that the minimal pressure $q_{\min}$ depended on h and on the granular material. In addition, phase (a) was associated with minor displacements in the bulk, a correlation between $q_{\min}$ and ϕ_p was assumed. Figure 32a gives $q_{\min}/\gamma_i$ versus ϕ_p for each numerical material tested. The experimental results obtained for sand and gravel layers 0.20 m thick are also shown in this figure. The lower ϕ_p was, the greater was the pressure on the trapdoor, i.e., the lower the load transfer was.

In addition, the three materials S_3, C_{20}^1 and C_{20}^1 with values for the peak friction angle ϕ_p between 35° and 37° gave very similar minimal pressures $q_{\min}$. The key parameter for the amplitude of load transfer during phase (a) was in this case ϕ_p, and no effect from the particle shape was observed on the load transfer and kinematics.

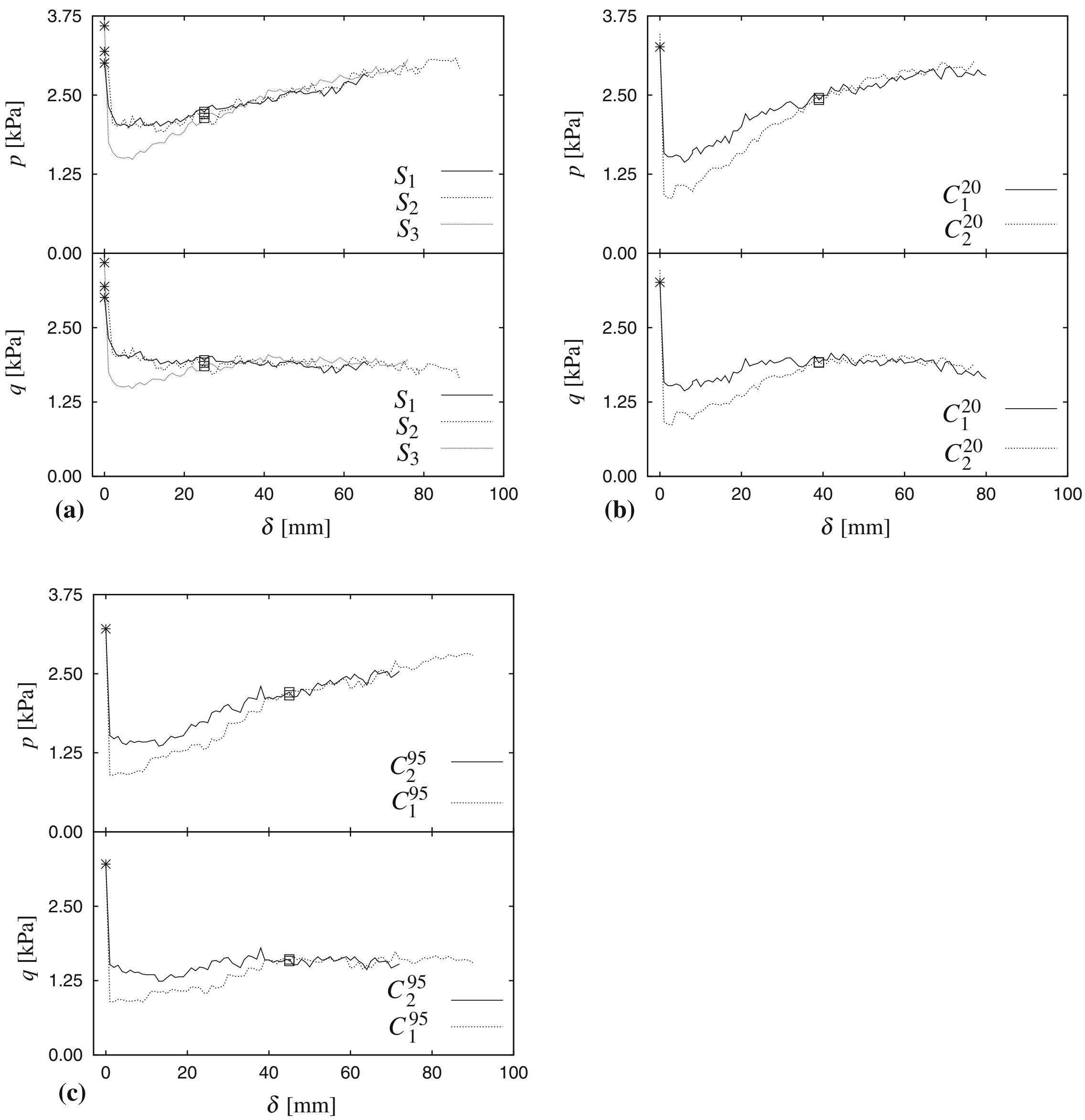

Fig. 29 Pressures (p and q) versus trapdoor displacement δ; the symbol *square* corresponds to the beginning of the critical phase ($h = 0.20$ m). **a** Spheres, **b** clusters 0.20d, **c** clusters 0.95d

The only influence of shape acts indirectly through the peak friction angle.

3.3.2 Phase (b)

After it reached its minimal value $q_{\min}$, pressure q increased rapidly and regularly with δ between 3 mm and 40 mm (Fig. 30—part b). At the end of phase (b), the pressure on the trapdoor reached a value of, q_c. In terms of kinematics, this phase corresponded to the expansion toward the surface of the previously formed wedge-shaped zone, as shown in Fig. 31b, c.

3.3.3 Phase (c)

Finally, pressure q reached a threshold (Fig. 30—part c). The boundaries of the slipping part of the granular material above the trapdoor consisted of two vertical planes starting at each edge of the trapdoor (Fig. 31d). This mechanism was very close to the one observed experimentally and also corresponded to the classical description of the phenomenon used in analytical models.

Phase (c) was associated with greater displacement values of the trapdoor, corresponding to substantial strains in the sample. In this case, a correlation between the

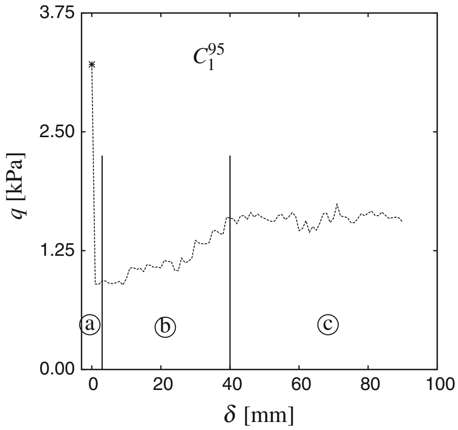

Fig. 30 Corrected pressure versus trapdoor displacement δ for material C_1^{95} ($h = 0.20$m)

corrected pressure q_c at the beginning of phase (c) and the critical friction angle, ϕ_c was assumed. Figure 32b shows q_c versus ϕ_c for all samples. Pressure q_c corresponding to the beginning of phase (c) slightly decreased with ϕ_c. Here, the effect of ϕ_c could not be disconnected from the effect of particle shape, since each particle shape S, C^{20} or C^{95} was associated with a unique value of ϕ_c.

3.4 Micromechanical analysis

The DEM gives a means to observe the mechanisms occurring at contact level between grains, in particular through displacement fields or local stress and strain tensors. It is possible to highlight numerous differences between the granular layers tested here with regard to the trapdoor problem. The influences of particle shapes and friction angles were investigated from a micro-mechanical point of view.

3.4.1 Calculation of stresses and strains in discrete particles assemblies

Stress tensors were calculated on volumes of constant size, each volume containing around 72 grains, all over the granular layer using Eq. 24. Each volume covered the whole width of the test box in the y-axis direction and was 2.5×2.5 mm in the xz plane and each volume contained between 170 and 320 contact points, depending on particle shape and porosity.

In terms of strain, the distributions of first and second invariants of strain tensors were calculated [8]. The network formed by the centers of mass of the particles was converted into an assembly of tetrahedrons. Between two successive configurations of the granular layer, the strain tensor for each tetrahedron can be written

$$\varepsilon_{ij} = \frac{1}{2}\left(\left\langle\frac{\partial u_i}{\partial j}\right\rangle + \left\langle\frac{\partial u_j}{\partial i}\right\rangle\right), \quad \text{with } i = x, y, z \quad \text{and} \quad j = x, y, z, \tag{25}$$

where $\mathbf{u}$ is the displacement field of the tetrahedron between the two configurations. The mean gradient of the displacement field $\mathbf{u}$ of the tetrahedron can be assessed by

$$\left\langle\frac{\partial u_i}{\partial j}\right\rangle = \frac{1}{V}\int_V \frac{\partial u_i}{\partial j}\mathrm{d}V \tag{26}$$

with V the volume of the tetrahedron. However, the Green-Gauss theorem gives

$$\int_V \frac{\partial u_i}{\partial j}\mathrm{d}V = \int_{\partial V} u_i n_j \mathrm{d}S \tag{27}$$

with n_j the normal exterior of the ∂V boundary of V. Assuming that the components of the displacement field $\mathbf{u}$ vary linearly between the vertex of the tetrahedron, the strain tensor of a tetrahedron between two configurations is given by

$$\varepsilon_{ij} = \frac{1}{2V}\sum_{\mathrm{k}}\left[\left(\int_S u_i \mathrm{d}S\right)n_j + \left(\int_S u_j \mathrm{d}S\right)n_i\right] \tag{28}$$

where k is the index of the faces of the tetrahedron.

3.4.2 Qualitative analysis of kinematics

The purpose here is to evaluate the possible effects of particle shapes and macro-mechanical shear resistance characteristics on the changes in orientation of the network of contact forces. The Fig. 33 shows the distribution of the normal components of contact forces in a sample made of C_3^{20}, for $\delta = 10$ mm (phase (a)). For a more accurate analysis of the mechanisms involved, the analysis of load transfer mechanisms was based on the distribution of shear strains and the principal stress directions. The analyses of phase (a) of maximal load transfer and of critical phase (c) are presented separately.

3.4.2.1 Case of phase (a) Three granular layers were chosen with different particle shapes for each and with similar peak friction angles ϕ_p and minimal pressure $q_{\min}$: S_3, C_1^{20} and C_1^{95}. Figure 34 shows the distribution of the second invariant of strain tensor $I_{2\varepsilon}$ and of the principal stress directions in the plane $(O, \mathbf{x}, \mathbf{z})$ for 3 materials in phase (a).

The distribution of $I_{2\varepsilon}$ and the principal stress directions both clearly revealed the arch pattern obtained due to trapdoor movement. The arch spanned the trapdoor and

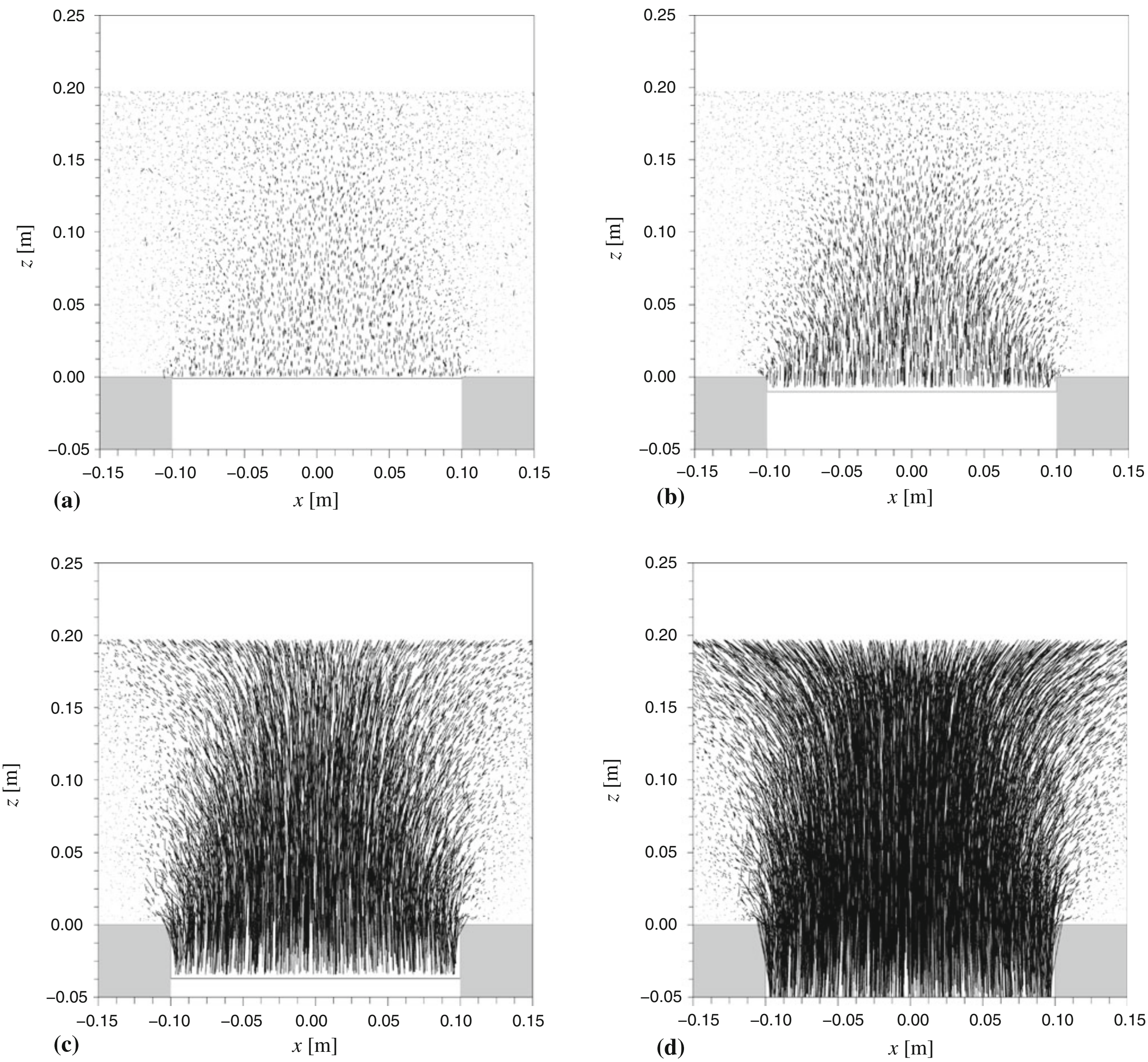

Fig. 31 Particle displacement fields in a vertical section of the layer for the numerical assembly C_1^{95}, for different values of trapdoor displacement δ in the $(\mathbf{x}, \mathbf{z})$ plan (for $\delta = 1$ mm, vector length is equal to 2.5 times particle displacement, 1 time for others) ($h = 0.20$m). **a** $\delta = 1$ mm, **b** $\delta = 10$ mm, **c** $\delta = 37$ mm, **d** $\delta = 62$ mm

stood on each side of the fixed part of the bottom of the test box. The arch followed the path formed by the directions of major principal stresses from one side of the trapdoor to the other. The path corresponded to strong shear strain zones. No significant differences could be found in the shape or width of the arches for these 3 materials. Therefore, for a given peak friction angle, no effect of particle shape was observed on the arch pattern.

Three other materials were then chosen, again with different particle shapes and peak friction angles ϕ_p. Figure 35 shows respectively the distributions of the second invariant of strain tensor $I_{2\varepsilon}$ and the principal stress directions in the plane $(O, \mathbf{x}, \mathbf{z})$ for the materials S_1, C_1^{95} and C_2^{20} in phase (a).

In Fig. 35, the arch pattern was still observable. However, for a lower value of ϕ_p, the arch was higher and its branches wider. In addition, the directions of principal stresses under the arch were not sorted. Contrary to this, for a higher value of ϕ_p, the arch was thinner and affected only the lower part of the granular layer: shear strain was more localized. In this case, the principal stress directions were properly sorted. Thus, the effect of the peak friction angle

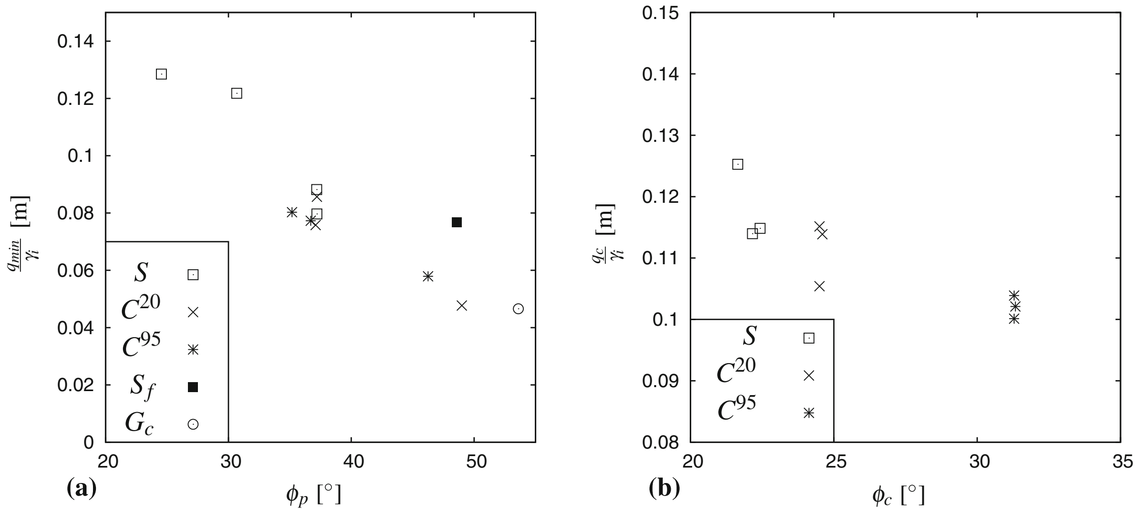

Fig. 32 Influence of the peak friction angle on ratio q/γ_i for all the samples for phases (*a*) and (*c*) (h = 0.20 m). **a** Phases (*a*) and **b** phase (*c*)

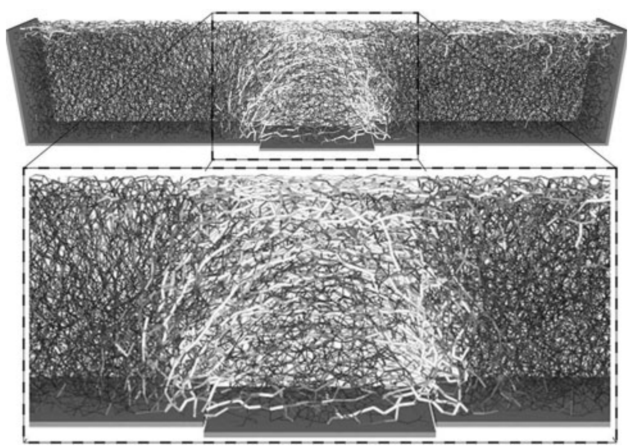

Fig. 33 Distribution of the normal contact forces f_n in the sample made of C_3^{20} particles. A *thin dark line* corresponds to a small value of f_n. A wide *white line* corresponds to a large value of f_n. Intermediate values of f_n are linearly distributed between thin to wide and *black* to *white lines*

on the arching mechanism was clearly identified for this phase.

3.4.2.2 Case of phase (c) As defined previously, the critical phase corresponds to the vertical sliding of the part of the granular layer located above the trapdoor. Phase (*c*) is associated with extensive displacements and strains in the granular layers. The friction mobilized in the granular layer is associated with the critical friction angle ϕ_c. For the materials presented here, ϕ_c depended on particle shape only. Consequently, the possible effects of particle shapes and ϕ_c could not be separated, as for phase (*a*). The comparison presented in this section was carried out with the following materials:

- S_1 and S_3: $\phi_c = 22°$,
- C_1^{20} and C_2^{20}: $\phi_c = 24.6°$,
- C_1^{95} and C_2^{95}: $\phi_c = 31.3°$.

Figure 36 shows the distributions of the values of the second invariant of strain tensor $I_{2\varepsilon} \geq 15\%$ in the $(O, \mathbf{x}, \mathbf{z})$ plane for a trapdoor displacement of $\delta = 59$ mm. The areas with the highest values of $I_{2\varepsilon}$ changed. The arch pattern was no longer observed. Two vertical shear bands developed at the edge of the trapdoor instead. From this point of view, the experimental observations agreed with the numerical modeling. The mechanism observed also corresponded to the classical analytical description of the trapdoor.

The shear localization pattern was very similar from one granular layer to the other. No significant differences could be observed based on particle shape or critical friction angle. The shear bands spread wider in the case of the material S_1 which corresponded to the lowest value of the peak friction angle value.

3.5 Correspondences with the analytical solution

In the experimental study, average stress on the trapdoor was predicted using the analytical solution of Eq. 1. It was shown that the required values of stress ratio K to be considered in order that a fairly good prediction of the average stress on the trapdoor was obtained were very far from the values recommended by some authors [40], such as the active earth pressure coefficient K_a.

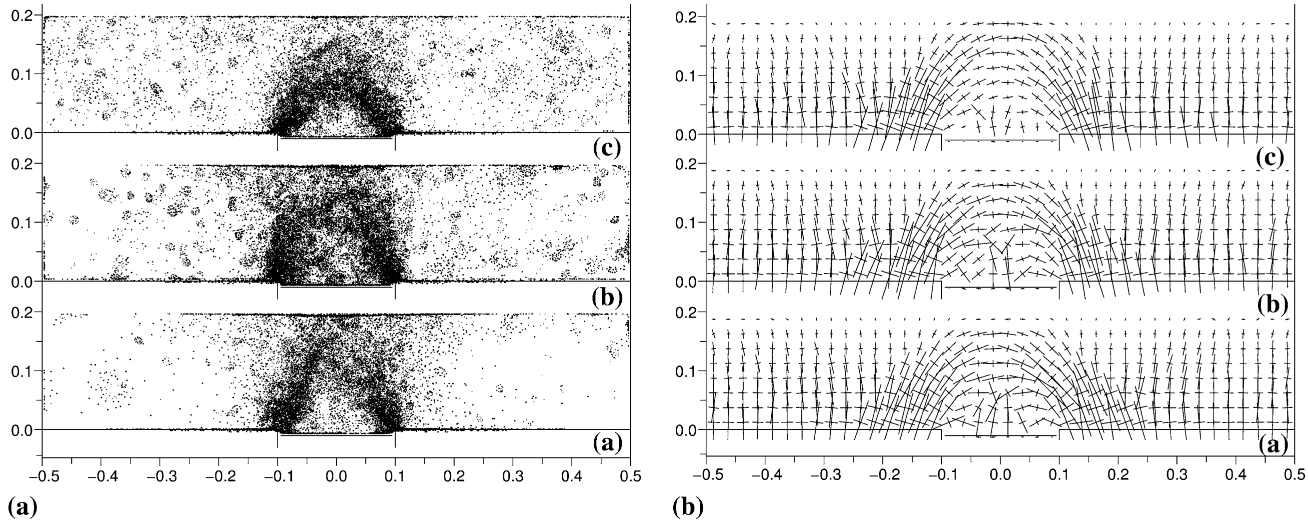

Fig. 34 Arch pattern for the maximal load transfer phase, for materials S_3 with $\phi_p = 37.1°$ (*a*), C_1^{20} with $\phi_p = 37.2°$ (*b*) and C_1^{95} with $\phi_p = 35.2°$ (*c*). **a** Second invariant of the strain tensor. **b** Principal stress directions

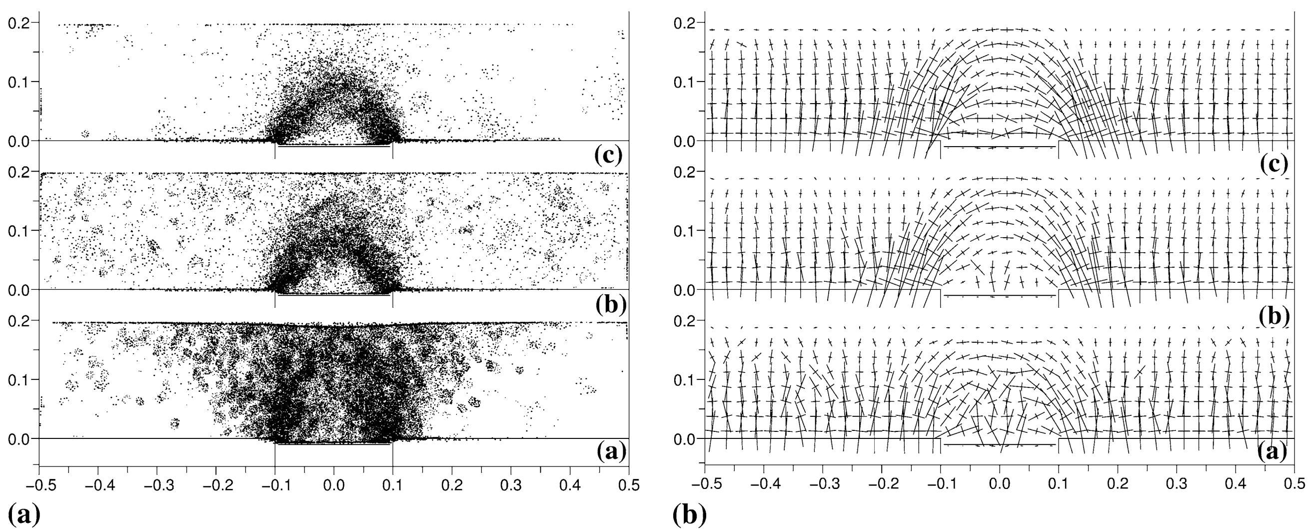

Fig. 35 Arch pattern for the maximal load transfer phase, for materials S_1 with $\phi_p = 24.5°$ (*a*), C_1^{95} with $\phi_p = 35.2°$ (*b*) and C_2^{20} with $\phi_p = 49.0°$ (*c*). **a** Second invariant of strain tensor. **b** Principal stress directions

In the numerical analyses, profiles of stress ratio K could be calculated with a micromechanical analysis. The ratio K of the horizontal stress to the vertical stress was calculated in the parallelepiped volumes described in Section 3.4.1.

The consistency of the stress ratios K was checked for two positions of the trapdoor. Profiles of K at the right and left ends of the test box were calculated. Figure 37 shows the profiles of K for material C_{20}^1 obtained for trapdoor displacements of $\delta = 10$ mm and $\delta = 59$ mm on the left-hand and right-hand ends of the test box. The profiles of K obtained were stationary as the trapdoor was moved; they were found to be consistent with the at rest earth pressure ratio proposed by Jaky [24]. The values of K obtained close to the top surface of the layer were much higher, consistent with the observations of Emam et al. [21].

The profiles of K were also calculated above each edge of the trapdoor. These parts of the granular layer corresponded to the shear bands which developed as the trapdoor moved downwards, as shown in Fig. 36. Figure 38 shows the profile of K along this direction for phase (*a*) and (*c*). Despite observation of some dispersion, the values of K obtained were relatively stationary as the depth changed and greater than 1.00 on average. In addition, the values of K increased as the trapdoor displacement increased.

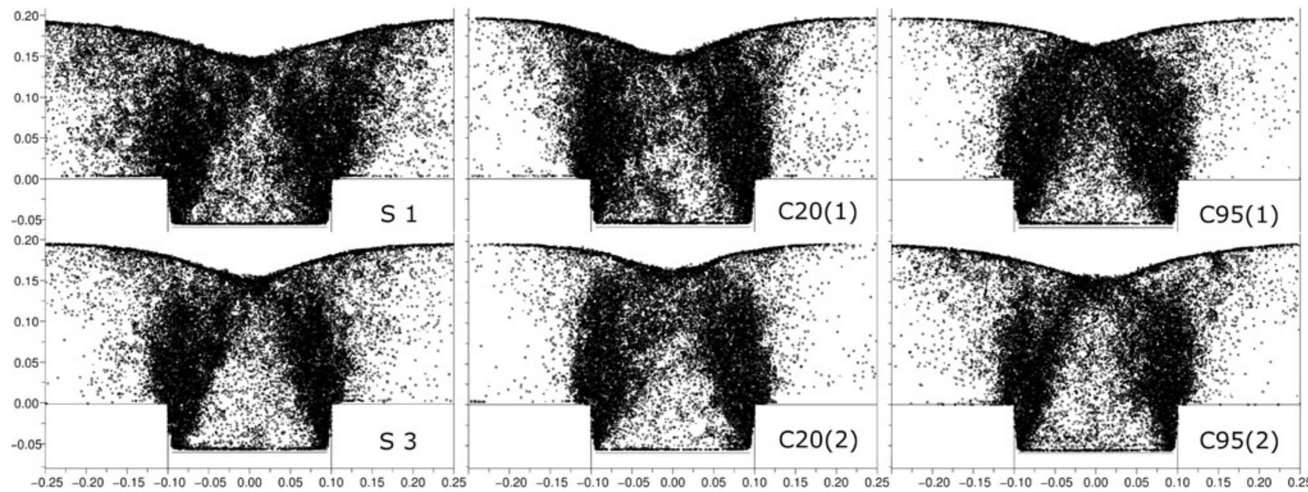

Fig. 36 Distributions of the second invariant of strain tensor $I_{2\varepsilon} \geq 15\%$ in the $(O, \mathbf{x}, \mathbf{z})$ plane for critical phase ($\delta = 59$mm)

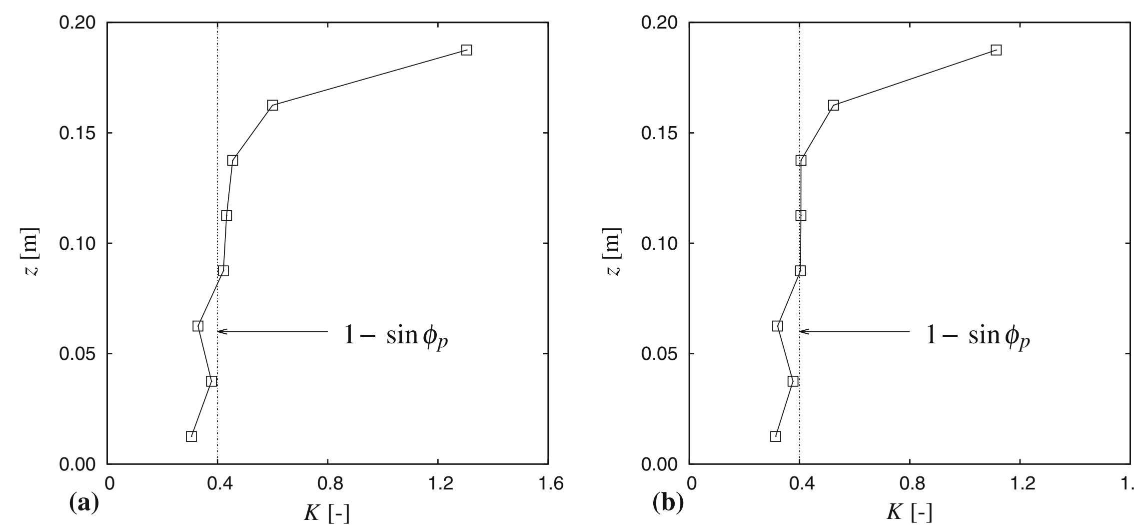

Fig. 37 Profile of average stress ratio K at *left* and *right* ends of the test box, versus the z-position (case of C_{20}^{1}; the *vertical dashed line* represents the at rest earth pressure ratio [24]). **a** $\delta = 10$ mm. **b** $\delta = 59$ mm

For each profile, an average value $\tilde{K}$ of $K(z_i)$ was calculated weighted by the corresponding mean stress $\tilde{\sigma}(z_i)$ at the considered depth z_i

$$\tilde{K} = \frac{\sum_{z_i} K(z_i)\tilde{\sigma}(z_i)}{\sum_{z_i} \tilde{\sigma}(z_i)} \tag{29}$$

The dispersion within the profile of $K(z_i)$ was estimated with the standard deviation weighted by the mean stress at the considered point.

Figure 39 shows the values of $\tilde{K}$ obtained for all the materials, versus the friction angle of the material: ϕ_p for $\delta = 10$ mm and ϕ_c for $\delta = 59$ mm. The values of $\tilde{K}$ ranged between 1.1 and 1.3. No relation could be found between the stress ratio $\tilde{K}$ and peak friction angles for the position of the trapdoor corresponding to phase (a). For $\delta = 59$ mm and phase $(c), \tilde{K}$ increased slightly as ϕ_c increased.

A prediction of the average stress on trapdoor q was computed with the values of $\tilde{K}$ using Eq. 1. Peak friction angle ϕ_p was used for the prediction of the stress for phase (a) and the critical friction angle ϕ_c for phase (c). The prediction results are shown in Fig. 40 and compared with the values obtained with numerical modeling and also with experimental testing. The prediction of the mean stress on the trapdoor was very good. The relation between friction angle ϕ and q obtained with numerical modeling was correctly reproduced.

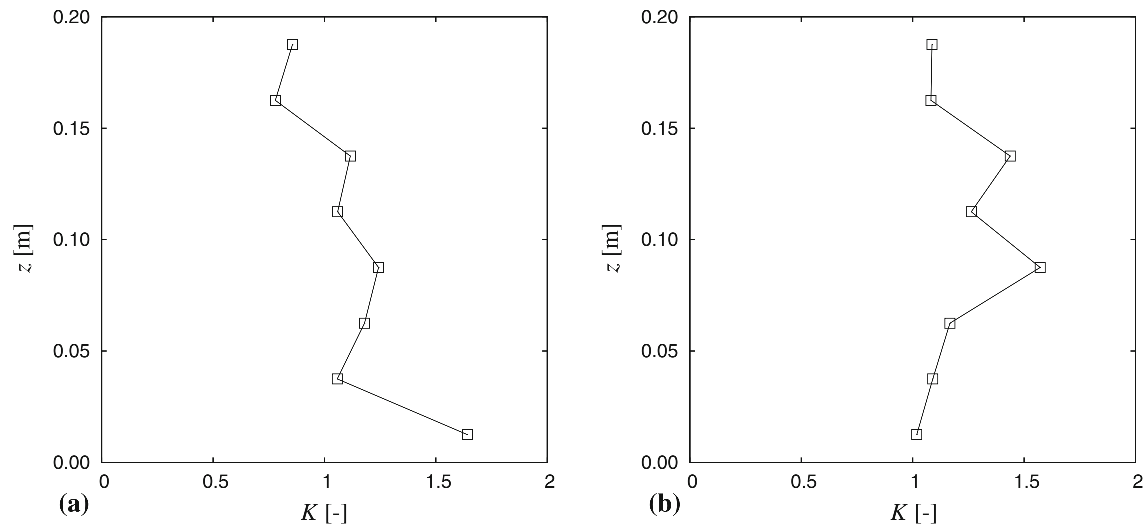

Fig. 38 Profile of stress ratio K at the edges of the trapdoor versus the z-position (case of C^1_{20}). **a** $\delta = 10$ mm. **b** $\delta = 59$ mm

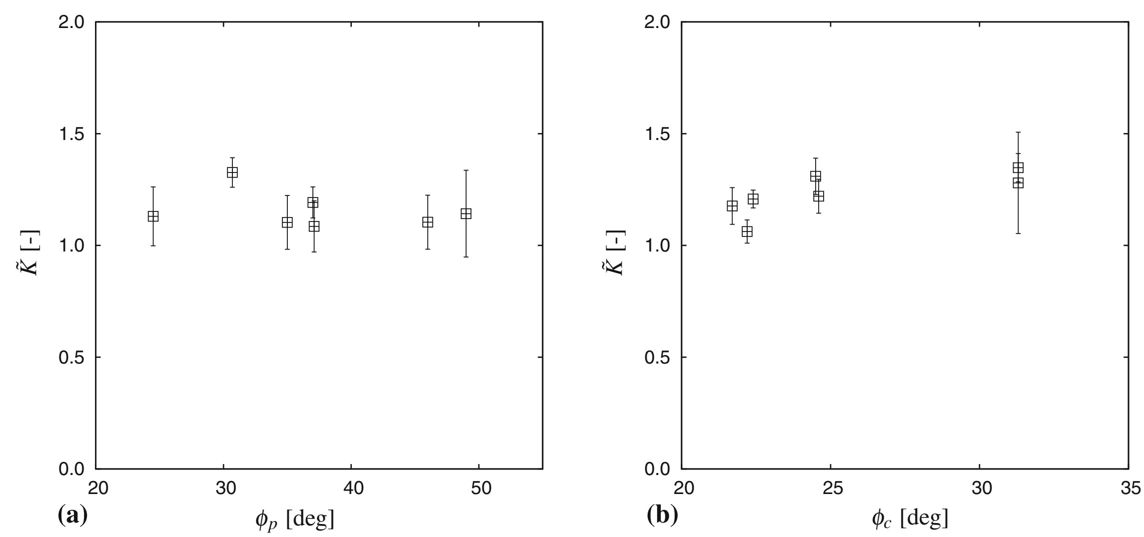

Fig. 39 Weighted mean stress ratio $\tilde{K}$ at the edges of the trapdoor versus the friction angle; error bars represent the weighted standard deviation on the profile. **a** $\delta = 10$ mm. **b** $\delta = 59$ mm

The analytical solution proposed by Terzaghi [40] gives satisfying results for both phases of the trapdoor as long as the value of stress ratio K is appropriately chosen. The active earth pressure coefficient could definitely not be used to predict the load transfers. The range of materials tested showed that the value of stress ratio K was not so dependent on the value of the friction angle and varied between 1.1 and 1.3.

3.5.1 Conclusion

The trapdoor test was accurately reproduced with the DEM. The response of the granular layers was divided into three successive phases, as described in the experimental study. A series of granular materials was modeled with similar particle size distribution. The friction angles of the materials were found to be the key parameters in the response of the granular layers. The first phase of maximal load transfer was clearly associated with the peak friction angle, while the critical phase was associated with the critical friction angle. The shape of particles influenced the values of the friction angle but for a given friction angle and different particle shapes, no differences were observed on the kinematics or on the amplitude of load transfers. Regarding the analytical solution of Terzaghi, the numerical modeling showed that the stress ratios K were very

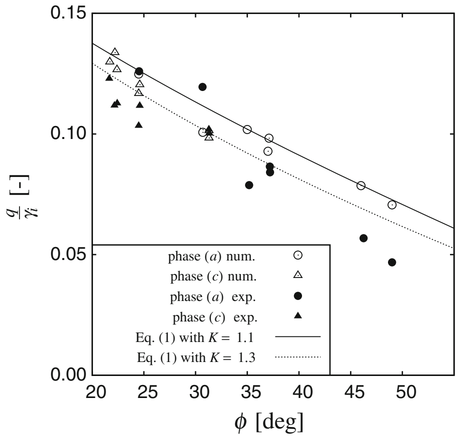

Fig. 40 Comparison of stress on trapdoor obtained with numerical model with predictions computed using analytical solution of Eq. 1 with stress ratios $\tilde{K}$ for phase (*a*) and (*c*)

close from one material to the other, and also greater than 1.00. Using such stress ratios, the mean stress of the trapdoor was satisfactorily predicted by the analytical solution.

4 Conclusion

The trapdoor problem involving granular materials was studied both experimentally and numerically. The experimental part was carried out with the use of two real geomaterials presenting high shear strength parameters. Differences existed between these two materials, particularly with regard to their particle size distribution. A substantial number of experimental trapdoor tests were conducted, involving different layer thicknesses: the ratio of the thickness to the trapdoor width varying from 1/4 to 3. The testing apparatus showed some limitations for the tests with the highest ratio, especially for extensive trapdoor displacements.

First, there were systematically 3 typical phases in the behavior of the granular layer. These three phases could be clearly identified in each test, despite the differences in materials:

- phase (*a*): occurring for very minor displacements of the trapdoor, corresponding to the maximal load transfers observed in the layer,
- phase (*b*): associated with a progressive expansion of the material above the trapdoor from the bottom to the top of the layer and with a gradual orientation of the failure plane starting from each edge of the trapdoor in a vertical direction,
- phase (*c*): corresponding to the classical description of the trapdoor problem: the volume of material located above the trapdoor slipping between the stable parts of the layers on each side of the trapdoor; the amplitude of load transfer during this phase tended to stabilize.

The pressure on the trapdoor resulting from the experimental tests was compared with the values obtained with the analytical solution of Terzaghi. The comparison showed that the ratio K between horizontal stress and vertical stress was a key parameter. Great differences in the response of both the materials tested showed that K cannot be deduced simply from classical earth pressure theory. Thus, a DEM study of the trapdoor problem was conducted, using experimental results as validation data for the numerical model.

In the numerical study, only one value of layer thickness was used in order to focus on the effect of the physical and mechanical parameters. The three phases of the response were observed. Load transfer amplitude of phases (*a*) and (*c*) were linked respectively to the peak and the critical friction angles of the materials. The variation of particle shapes had a great influence on the macro-mechanical parameters and shear strength in particular. In fact, particle shape influenced indirectly the response of the layer. However, layers with different particle shapes and similar shear strength presented similar behavior during tests.

A micro-mechanical analysis was performed in order to investigate the localization of the shear strains and the distributions of stresses. During phase (*a*), an arch pattern developed above the trapdoor: as soon as the trapdoor was moved, the force paths were immediately re-oriented toward stable areas. The height and width of the arch pattern decreased as the peak friction angle increased. Phase (*c*) corresponded to a mechanism similar to the classical description of the trapdoor problem: the whole height of the layer above the trapdoor was affected by the displacement of the latter. The disturbance was concentrated above each edge of the trapdoor. As the critical friction angle increased, the width of the shear bands decreased. No direct influence of particle shape on the mechanisms was observed.

Finally, the stress ratios K were calculated along the vertical planes starting at each edge of the trapdoor. The stress ratios K ranged between 1.0 and 1.3 for all the materials, and for both phase (*a*) and (*c*). Considering the range of peak and critical friction angles involved, these variations of K could be considered minimal. Predictions of the stresses on the trapdoor with the analytical solution of Terzaghi were computed using the peak friction angle for phase (*a*), the critical friction angle for phase (*c*) and the values of K obtained previously. The correlation between prediction and numerical results was very good.

In conclusion, trapdoor displacement greatly influences load transfer amplitude. Load transfers can be fairly well estimated with the analytical solution of Terzaghi. In this solution, the amplitude of trapdoor displacement must be considered within the friction angle of the material: peak friction angle for minor displacements and critical friction angle for greater displacements. For parameter K, values between 1.0 and 1.3 were obtained in this particular study, but these values corresponded to specific particular particle size distributions. However, it was confirmed by both experimental and numerical studies that K cannot be deduced from earth pressure theory.

Moreover, the numerical study focused on a single value of the thickness of the granular layer, for which the whole thickness was mobilized by the procedure: this may not be necessarily true for thicker layers. Consequently, further study should focus on the effect of particle size distribution and on the thickness of the granular layer.

Acknowledgments The authors would like to acknowledge the technicians of the Civil Engineering department of the IUT1/UJF-Grenoble with special thanks to H. Orand who designed and build the Trap door experimental apparatus. The authors also would like to express their gratitude toward C. Thornton at University of Birmingham for their helpful discussions.

References

1. AASHTO (2007) AASHTO LRFD bridge design specifications, S.I. units, 4th edn. American Association of State Highway and Transportation Officials
2. Agnolin I, Roux JN (2007) Internal states of model isotropic granular packings. III. Elastic properties. Phys Rev E 76(6): 061304
3. Allen M, Tildesley D (1994) Computer simulation of liquids. Oxford University Press, Oxford
4. Atman APF, Brunet P, Geng J, Reydellet G, Combe G, Claudin P, Behringer RP, Clément E (2005) Sensitivity of the stress response function to packing preparation. J Phys Condens Matter 17(24):S2391
5. Atman APF, Claudin P, Combe G (2009) Departure from elasticity in granular layers: investigation of a crossover overload force. Comput Phys Commun 180:612–615
6. Bathurst J, Rothenburg L (1988) Micromechanical aspects of isotropic granular assemblies with linear contact interactions. J Appl Mech 55(1):17–23
7. Briançon L, Villard P (2008) Design of geosynthetic-reinforced platforms spanning localized sinkholes. Geotext Geomembr 26(5):416–428
8. Calvetti F, Combe G, Lanier J (1997) Experimental micromechanical analysis of a 2D granular material: relation between structure evolution and loading path. Mech Cohes Frict Mater 2:121–163
9. Chareyre B, Villard P (2005) Dynamic spar elements and DEM in 2-dimensions for the modelling of soil-inclusion problems. J Eng Mech ASCE 131(7):689–698
10. Chevalier B, Combe G, Villard P (2007) Study of the mechanical behavior of heterogeneous granular materials by means of distinct element method. Bull des Laboratoires des Ponts et Chaussées 268(269):105–128
11. Chevalier B, Combe G, Villard P (2009) Experimental and numerical study of the response of granular layer in the trap-door problem. In: Nakagawa M, Luding S (eds) Powders and grains 2009. American Institute of Physics, Melville, New York, pp 649–652. doi:10.1063/1.3180010
12. Chevalier B, Villard P, Combe G (2011) Investigation of load transfer mechanisms in geotechnical earth structures with thin fill platforms reinforced by rigid inclusions. Int J Geomech 11(3):12. doi:10.1061/(ASCE)GM.1943-5622.0000083
13. Combe G (2002) Mécanique des matériaux granulaires et origines microscopiques de la déformation. études et Recherches du Laboratoire Central des Ponts et Chaussées
14. Combe G, Roux JN (2000) Strain versus stress in a model granular material: a devil's staircase. Phys Rev Lett 85:3628–3631
15. Combe G, Roux JN (2003) Discrete numerical simulation, quasistatic deformation and the origin of strain in granular materials. In: Di Benedetto et al. (eds) 3ème Symp. Int. sur le Comportement des sols et des roches tendres, Lyon, pp 1071–1078
16. Combe G, Roux JN (2011) Discrete-element modeling of granular materials. Chap 6: construction of granular assemblies under static loading. ISTE Ldt and Wiley, London, pp 153–179
17. Cundall P, Strack ODL (1979) A discrete numerical model for granular assemblies. Géotechnique 29:47–65
18. Cundall PA, Dresher A, Strack ODL (1982) Numerical experiments on granular assemblies: measurements and observations. In: IUTAM conference on deformation and failure of granular materials. Delft
19. Deutsche Gesellschaft für Geotechnik (1997) Empfehlungen für Bewehrungen aus GEOkunststoffen: Bewehrte Erdkörper auf punkt- oder linienförmigen Traggliedern
20. Donzé FV, Magnier SA (1995) Formulation of a three dimensional numerical model of brittle behavior. Geophys J Int 122:790–802
21. Emam S, Roux J-N, Canou J, Corfdir A, Dupla J-C (2005) Granular packings assembled by rain deposition: an experimental and numerical study. In: García Rojo R, Herrmann H, McNamara S (eds) Powders and grains 2005, vol 1. Balkema, Leiden, Netherlands, pp 49–52
22. Emeriault F, Cambou B, Mahboudi A (1996) Homogenization for granular materials: non reversible behaviour. Mech Cohes Frict Mater 1:199–218
23. Handy RL (1985) The arch in soil arching. J Geotech Eng 111(3):302–318
24. Jaky J (1944) The coefficient of earth pressure at rest. J Soc Hung Arch Eng 78(22):355–358
25. Janssen HA (1895) Versuche über Getreidedruck in Silozellen. Zeitung des Vereins deutscher Ingenieure 39:1045
26. Kolb E, Mazozi T, Clément E, Duran J (1999) Force fluctuations ina vertically pushed granular column. Eur Phys J B 8:483–491
27. Lancelot L, Shahrour I, Al Mahmoud M (2006) Failure and dilatancy properties of sand at relatively low stresses. J Eng Mech 132(12):1396–1399
28. Le Hello B, Villard P (2009) Embankments reinforced by piles and geosynthetics numerical and experimental studies dealing with the transfer of load on the soil embankment. Eng Geol 106:78–91
29. Marston A, Anderson AO (1913) The theory of load on pipes ditches and test of cement and clay drain tile and sewer pipes, Rapport technique 31. Iowa State College, Iowa
30. McKelvey JA III (1994) The anatomy of soil arching. Geotext Geomembr 13:317–329
31. Moreau JJ, Jean M (1992) Unilaterality and granular friction in the dynamics of rigid body collections. In: Curnier A (ed) Proceedings of the contact mechanics international symposium. Presses Polytechniques Universitaires Romandes, Lausanne, pp 31–48
32. Papamichos E, Vardoulakis I, Heil LK (2001) Overburden modeling above a compacting reservoir using a trap door apparatus. Phys Chem Earth A 26(1–2):69–74

33. Rankine WJM (1857) On the stability of loose earth. Philos Trans R Soc Lond 147:9–27
34. Roscoe HK (1970) The influence of strain in geomechanics. Géotechnique 20:129–170
35. Roux JN, Chevoir F (2005) Simulation numérique discrète et comportement mécanique des matériaux granulaires. Bull des Laboratoires des Ponts et Chaussées 254:109–138
36. Salot C, Gotteland P, Villard P (2009) Influence of relative density on granular materials behavior: DEM simulations of triaxial tests. Gran Matter 11(4):221–236
37. Schäfer S, Dippel S, Wolf D (1996) Forces schemes in simulations of granular materials. Journal de physique I 6(1):5–20
38. Szarf K, Combe G, Villard P (2009) Influence of the grains shape on the mechanical behavior of granular materials. In: Nakagawa M, Luding S (eds) Powders and grains 2009. American Institute of Physics, Melville, New York, pp 357–360
39. Szarf K, Combe G, Villard P (2011) Polygons vs. clumps of discs: a numerical study of the influence of grain shape on the mechanical behaviour of granular materials. Powder Technol 208(2):279–288
40. Terzaghi K (1936) Stress distribution in dry and saturated sand above a yielding trap-door. In: Proceedings of international conference of soil mechanics, vol. 1. Harvard University, Cambridge, pp 307–311
41. Terzaghi K (1943) Theoretical soil mechanics. Wiley, London
42. Vardoulakis I, Graf B, Gudehus G (1981) Trap-door problem with dry sand: a statical approach based upon model test kinematics. Int J Num Anal Methods Geomech 5:57–78
43. Villard P, Chevalier B, Le Hello B, Combe G (2009) Coupling between finite and discrete element methods for the modelling of earth structures reinforced by geosynthetic. Comput Geotech 36(5):709–717. doi:10.1016/j.compgeo.2008.11.005
44. Walker DM (1966) An approximate theory for pressures and arching in hoppers. Chem Eng Sci 21:975–997
45. Walters JK (1973) A theoretical analysis of stresses in silos with vertical walls. Chem Eng Sci 28:13–21
46. Weber J (1966) Recherches concernant les contraintes intergranulaires dans les milieux pulvérulents. Bull de Liaison des Ponts et Chaussées 20